

Important note: This is the originally submitted version. Readers are advised to refer to the final version, available free of charge at <http://dx.doi.org/10.1007/s00382-012-1316-1> with the following reference: B. De Saedeleer, M. Crucifix, S. Wiczorek, Is the astronomical forcing a reliable and unique pacemaker for climate? A conceptual model study, *Climate Dynamics*, (2013) 40:273–294.

Is the astronomical forcing a reliable and unique pacemaker for Climate?

by

BERNARD DE SAEDELEER[†]

MICHEL CRUCIFIX[†]

SEBASTIAN WIECZOREK[‡]

[†] *Georges Lemaître Centre for Earth and Climate Research,
Université catholique de Louvain, Louvain-la-Neuve, Belgium*

[‡] *University of Exeter, Exeter, UK*

Abstract

There is evidence that ice age cycles are paced by astronomical forcing, suggesting some kind of synchronization phenomenon. Here, we identify the type of such synchronization and explore systematically its uniqueness and robustness using a simple paleoclimate model akin to the Van der Pol relaxation oscillator and dynamical system theory. As the insolation is quite a complex quasiperiodic signal, the traditional concepts of phase- or frequency-locking used to define synchronization to periodic forcing are inadequate. Instead, we explore a different concept of *generalized synchronization* in terms of (coexisting) synchronized solutions for the forced system, their basins of attraction and instabilities.

We propose a clustering technique to compute the number of synchronized solutions, each of which corresponds to a different paleoclimate history. In this way, we uncover multistable synchronization (reminiscent of phase- or frequency-locking to individual periodic components of astronomical forcing) at low forcing strength, and monostable or unique synchronization at stronger forcing. In the multistable regime, different initial conditions may lead to different paleoclimate histories. To study their robustness, we analyze Lyapunov exponents that quantify the rate of convergence towards each synchronized solution (local stability), and basins of attraction that indicate critical levels of external perturbations (global stability). We find that even though synchronized solutions are stable on a long term, there

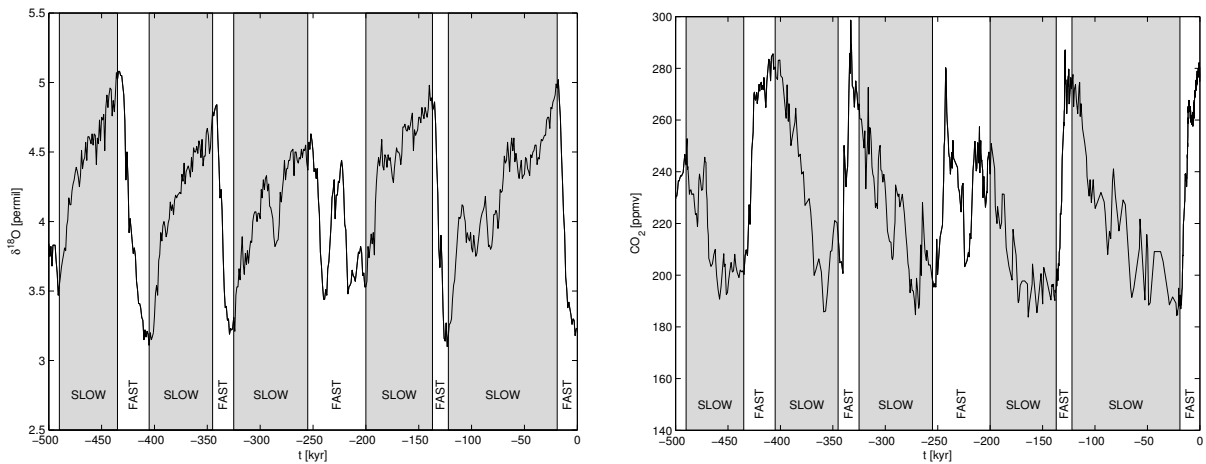
exist short episodes of desynchronization where nearby climate trajectories diverge temporarily (for about 50 kyr). We also show that when a synchronized solution approaches the boundary of its basin of attraction, small perturbations may cause a jump to a different (coexisting) paleoclimate history.

Our study brings new insight into paleoclimate dynamics and reveals a possibility for the climate system to wander throughout different climatic histories related to preferential synchronization regimes on obliquity, precession or combinations of both, as environmental parameters varied throughout the history of the Pleistocene.

Keywords : Climate Models Milankovitch Oscillator Generalized Synchronization Lyapunov exponent

1 Introduction

This article is a contribution to the field of paleoclimate dynamics theory, which has experienced many developments in terms of ice age models since many years notably by [Le Treut and Ghil, 1983, Saltzman and Maasch, 1990], and many others, and remains an active research field. Paleoclimate modeling is a complex problem, hence an uncomfortable situation for a scientist. On one hand, the data are scarce and marred by uncertainties. On the other hand, there is not a single well established model, the problem is non autonomous, the forcing is aperiodic, and stochastic ef-



(a) The LR04 stack [Lisiecki and Raymo, 2005] of 57 benthic $\delta^{18}O$ [‰] records; the $\delta^{18}O$ is a proxy for the global volume of ice. High values of $\delta^{18}O$ correspond to a colder climate (glacial state).

(b) CO_2 composite record [ppmv] [Luethi et al., 2008]. High values of CO_2 correspond to a warmer climate (interglacial state).

Figure 1: The long-term climatic signals reveal a slow-fast dynamics (only the most recent 500 kyr of the data are displayed here). The areas in grey (width τ_{slow}) are wider than the areas in white (width τ_{fast}): while glaciation is a slow process of ice build-up, deglaciation occurs much more rapidly ($\tau_{slow} > \tau_{fast}$). One also recognizes the last deglaciation which started some 20 kyr ago, up to the present time ($t = 0$).

fects are present.

Here, we focus on the slow variations of climate over the few last million years, which include the phenomenon of ice ages [Hays et al., 1976], that is, the repeated growth and decay of ice sheets in the Northern Hemisphere of a total mass as big as modern Antarctica's. When examining long-term climatic signals like the 5.3 Myr-long stack produced in [Lisiecki and Raymo, 2005], or the 800 kyr-long EPICA Dome C Ice Core from [Luethi et al., 2008], plotted respectively in Fig. 1(a) and Fig. 1(b) for the last 500 kyr, one immediately identifies three clearly visible features of the climatic time series:

- (i) *oscillations*: the signal oscillates between higher and lower values of ice volume corresponding to the glacial and interglacial states,
- (ii) *asymmetry*: in Fig. 1(a) typical transitions from a minimum to a maximum take much longer than transitions from a maximum to a minimum: deglaciations occur much more rapidly ($\tau_{fast} \approx 10$ kyr) than glaciations ($\tau_{slow} \approx 80$ kyr), giving a distinctive saw-tooth structure in the glacial/interglacial (G/I) cycles, especially pronounced over the last 500 kyrs,

- (iii) *100-kyr dominant period*: this has been identified by many authors since [Broecker and van Donk, 1970]. Note that the G/I cycles are not periodic.

The asymmetry in the oscillations has been studied by many authors. In order to reproduce it, some authors use underlying physical principles to build phenomenological models that exhibit slow-fast dynamics reasonably mimicking the climatic proxies [Saltzman, 2002]. Others assume this asymmetry by explicitly defining 2 different parameters such as the time intervals $\tau_{up} = \tau_{slow}$ and $\tau_{down} = \tau_{fast}$ [Ashkenazy, 2006] or time constants (τ_R and τ_F in [Paillard, 1998] and T_w and T_c in [Imbrie and Imbrie, 1980]). Whatever the model, it has to ultimately exhibit bimetric oscillations under the effect of the forcing, as it is aimed to mimic the oscillations between G/I states. Relaxation oscillators are therefore very straightforward natural candidates of ice age models. In this article, we will consider a slightly modified van der Pol oscillator model to illustrate the new contributions of our synchronization concepts.

In this paper, we concentrate on the influence of the astronomical forcing on Earth's climate. This forcing is induced by the slow variations in the spatial and seasonal distributions of incoming solar radiation (insola-

tion) at the top of the atmosphere, associated with the slow variations of the Earth's astronomical elements: eccentricity (e), true solar longitude of the perihelion measured with respect to the moving vernal equinox (ϖ), and Earth obliquity (ε_E). These quantities are now accurately known over several tens of millions of years [Laskar et al., 2004], but analytical approximations of e , $e \sin \varpi$, and ε_E valid back to one million years have been known since [Berger, 1978]. They take the form of d'Alembert series ($\sum A_i \sin[\omega_i t + \phi_i]$).

The external forcing $F(t)$ used throughout this article is the insolation at 65°N latitude on the day of the summer solstice. That specific insolation quantity is commonly related to the Milankovitch theory and can be thought of as a measure of how much ice may melt over summer. It can be written under the following compact form:

$$F(t) = \sum_{i=1}^{35} [s_i \sin(\omega_i t) + c_i \cos(\omega_i t)] \quad (1)$$

where the value of the 3×35 parameters (including ω_i , s_i , and c_i) are given in the Table 1 of Appendix A. The coefficients were extracted from [Berger, 1978] by performing a linear regression of the insolation on the ω_i . The validity range of this approximation is $[-1 \text{ Myr}, 0 \text{ Myr}]$, and its mean error (mean of the absolute value of the difference, compared to [Laskar et al., 2004]) is 6.7 W/m^2 with peaks at 27.5 W/m^2 . Note that the mean value (494.2447 W/m^2) has been removed; the theoretical framework that allows to work with anomalies was justified by [Saltzman and Maasch, 1991]. In short, this can be done as we are interested in oscillations, and not in the mean values themselves. The *quasiperiodic*¹ nature of the insolation forcing $F(t)$ is illustrated in its spectrum decomposition in Fig. 2. Precession is dominated by two harmonics around 19 and 23 kyrs (1 kyr = 1,000 years) and obliquity is dominated by an harmonic with a period of 41 kyrs but it bears periods as long as 1,200 kyrs.

Synchronization

There is ample evidence that the astronomical forcing influences the climate system. The phrase 'pacemaker of ice ages' was coined in a seminal paper [Hays et al., 1976] to express the idea that the timing of ice ages is controlled by the astronomical forcing.

¹ A *quasiperiodic* signal is the superposition of several periodic signals with incommensurate periods.

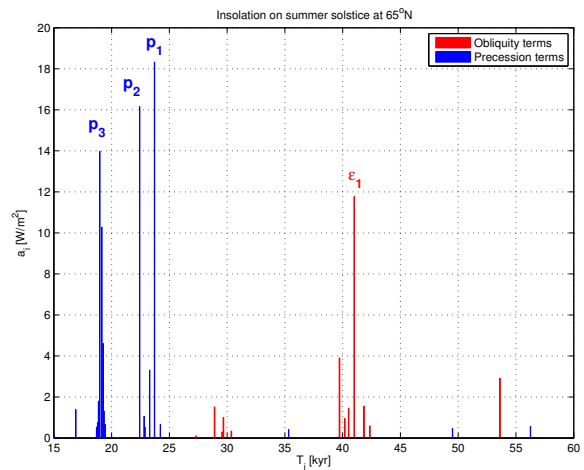


Figure 2: Spectrum decomposition of the incoming solar radiation (insolation) at 65°N latitude on the day of the summer solstice ($F(t)$ given in Eq. (1)). This is a graphical representation of Table 1 in Appendix A, with $a_i^2 = s_i^2 + c_i^2$ and $T_i = 2\pi/\omega_i$. The eight largest parameters a_i , which represent already 80% of the signal, are the major components of the insolation; they clearly come from the precession (19 and 23 kyr), and from the obliquity (41 kyr) associated series. This insolation is the forcing used to construct all Figures subject to the quasiperiodic astronomical forcing. The main harmonic ε_1 associated with obliquity has an angular velocity $\omega_{\varepsilon_1} = 0.1532 \text{ rad/kyr}$ ($T_{\varepsilon_1} = 41.0 \text{ kyr}$) and an amplitude of $a_{\varepsilon_1} = 11.77 \text{ W/m}^2$. The three main harmonics associated with precession are denoted p_1 , p_2 and p_3 .

while the ice age cycle itself is shaped by internal system dynamics. The paradigm has prevailed since then and is it still supported by the most recent analyses of palaeoclimate records [Lisiecki and Raymo, 2007, Huybers, 2007]. The notion of ‘pacemaker’ naturally evokes some sort of synchronization. However, despite some attempts, the actual type of synchronization has not been clearly identified or demonstrated to date. For example, [Ashkenazy, 2006, Tziperman et al., 2006] speak of “nonlinear phase-locking” although they do not define suitable “phase variables” that can be used to demonstrate a fixed-in-time relationship between phases of the forcing and the oscillator response.

Synchronization, as a universal nonlinear phenomenon, is a pervasive process in Nature, as it is associated with rhythmic processes. It is therefore not surprising to have synchronization also in Paleoclimatic Sciences. Depending on the forcing type (periodic, chaotic, stochastic), one can distinguish many types of synchronization including complete, lag, phase, frequency, identical, generalized [Rulkov et al., 1995], achronal and isochronous [Wu et al., 2006], and even noise synchronization. For a review, the reader is referred to [Balanov et al., 2009, Pikovsky et al., 2001], among others. While some terminology is still debated, [Brown and Kocarev, 2000] proposed an unified definition of synchronization for dynamical systems—there is synchronization if there exists a relationship h between the measured properties of the forcing, $g(\vec{u})$, and those of the oscillator, $g(\vec{v})$:

$$h(g(\vec{u}), g(\vec{v})) = 0, \quad (2)$$

that is fixed-in-time, meaning that h is time independent. Because we are interested in synchronization that is stable, for arbitrary initial conditions $\vec{u}(0)$ and $\vec{v}(0)$ that do not satisfy (2), we require that [Brown and Kocarev, 2000]:

$$\lim_{t \rightarrow \infty} h(g(\vec{u}(t)), g(\vec{v}(t))) = 0. \quad (3)$$

For example, if $g(\vec{u}) = \vec{u}$, $g(\vec{v}) = \vec{v}$, \vec{u} and \vec{v} have the same dimension, and (2) can be written as $\vec{u} = \vec{v}$, we speak of *identical synchronization*. More generally, if vectors \vec{u} and \vec{v} have different dimensions and (2) cannot be reduced to more than a functional relationship $\vec{u} = H(\vec{v})$, we speak of *generalized synchronization*; see also [Abarbanel et al., 1996, Rulkov et al., 1995, Pikovsky et al., 2001]. Note that the relationship (2)

need not be unique. If there are two or more relationships (2) for the same parameter settings, we speak of *multistable synchronization* [Pikovsky et al., 2001, Ch.15.3.2]. Then, which of the relationships the system settles to will depend on initial conditions.

In this paper, we use a simple van der Pol oscillator model to identify and illustrate for the first time the phenomenon of generalized synchronization between ice age cycles and astronomical forcing. The dynamical systems approach outlined in the next section (i) allows for stability analysis of such synchronization, (ii) uncovers interesting effects relating to the robustness of the synchronization with respect to external perturbations, and (iii) uncovers the phenomenon of multistable synchronization that has been overlooked by previous studies. We show that, in contrast to claims in [Tziperman et al., 2006], synchronization needs not be unique.

The article is structured as follows. Section 2 introduces a slightly modified version of the van der Pol oscillator as a suitable model for studying synchronization of ice ages to astronomical forcing. In Section 3, we analyse synchronization to periodic forcing and quasiperiodic astronomical forcing in terms of largest Lyapunov exponents. Section 4 is dedicated to the study of multistable synchronization in terms of attracting trajectories in the phase space of the forced system, and the associated basins of attraction. In Section 5, we investigate effects of the symmetry-breaking parameter β for the van der Pol oscillator model. Section 6 is concerned with the robustness of the synchronization and focuses on two aspects relating to predictability. Firstly, it shows that the local stability can be lost temporarily causing divergence of nearby climatic trajectories. Secondly, it demonstrates that in the multistable regime external perturbations (such as noise) may cause jumps between coexisting synchronized solutions when these solutions come close to their basin boundary. To be clear, all the treatment below is deterministic, except for Figs. 14 and 16.

This article requires some basics of Dynamical Systems theory (dynamical systems, nonlinear oscillations, limit cycles, bifurcations of vector fields, etc.), for which we refer the reader to [Guckenheimer and Holmes, 1983, Arnold, 1983, Strogatz, 1994], to [Saltzman, 2002] for dynamical paleoclimatology, and also to [Savi, 2005] for a review of some useful concepts.

2 Generic ice age model: a modified van der Pol relaxation oscillator

The hypothesis at the basis of the work by Milankovitch [Milankovitch, 1941] is that changes in total amount of continental ice (say: x) are driven by summer insolation $F(t)$ already described in Eq. (1). One straightforward interpretation of this hypothesis is a simple differential equation $\dot{x} = -d\Psi(x)/dx - \gamma F(t)$, where $d\Psi(x)/dx$ is the derivative of a climatic potential and γ is the *forcing efficiency*. However, models of this form fail in practice to correctly capture the rapid deglaciation phenomenon. We therefore propose to model the paleoclimatic dynamical system with a dissipative self-sustained oscillator resembling the classical van der Pol oscillator²:

$$\tau \dot{x} = -[y + \beta - \gamma F(t)] \quad (4a)$$

$$\tau \dot{y} = -\alpha [\Phi'(y) - x] \quad (4b)$$

where $\Phi'(y) = y^3/3 - y$. Note that this system is nonautonomous because the right-hand side depends explicitly on time.

The physical interpretation of the model is as follows. Ice volume x integrates the external forcing $F(t)$ over time but with a drift $y + \beta$. Assuming $\alpha \gg 1$, y is the faster variable whose dynamics is controlled by a two-well potential $\Phi(y)$. For example, there are arguments that the dynamics of the Atlantic ocean circulation may be approximated by an equation similar to Eq. 4b [Rahmstorf et al., 2005, Dijkstra et al., 2003]. Further interpretation and discussion of the fast variable can be found in [Saltzman et al., 1984, Tziperman and Gildor, 2003, Paillard and Parrenin, 2004, Tziperman et al., 2006, Crucifix, 2011]. The parameter τ sets the slow time scale. The coupled system Eq. (4) has one stable equilibrium solution for $|\beta| > 1$ and a stable periodic orbit for $|\beta| < 1$. The ratio of time spent near the two stable branches of the slow manifold given by $\Phi'(y) = x$ depends on β (see the paragraph "Time Spent" in Appendix B). We use T_{ULC} to denote the period of the stable periodic orbit and $\omega_{ULC} = 2\pi/T_{ULC}$ to denote the corresponding angular velocity.

Relaxation oscillators have been proposed previously to study ice ages [Saltzman et al., 1984, Tziperman and Gildor, 2003,

Paillard and Parrenin, 2004] although, to our knowledge, in a less general form than here. We adopted this form³ because it is very close to the well-studied van der Pol oscillator, and a good agreement (timing of glaciations and deglaciations, and their amplitude) with ice volume proxies was easily found for well chosen values of α, β, γ and τ (Fig. 3). We note, though, that small changes in parameters or additive fluctuations may easily shift the timings of ice-age terminations for reasons that will be clarified later in the paper.

The definition of synchronization can be applied to our model Eq. (4) as follows. The astronomical forcing $F(t)$ corresponds to $\vec{u}(t)$, and the state vector whose two components are the slowly-varying ice volume x and the faster variable y corresponds to $\vec{v}(t)$. For nonperiodic forcing, relationship (2) can be very complicated (non-functional or even fractal-like) and hence difficult to detect. Therefore, other methods of detecting (2) had to be developed. As suggested by the auxiliary system approach [Abarbanel et al., 1996], relationships (2) and (3) are implied by an (invariant) *attracting trajectory* in the (x, y, t) phase space of the nonautonomous forced system (4) [Wieczorek, 2011]. In the remainder of the paper, such an attracting trajectory is denoted with AT and referred to as an *attracting climatic trajectory* or *synchronized solution*. All other solutions to Eq. (4) will be referred to as *climatic trajectories*.

Previous approaches to nonlinear dynamics of quasiperiodically forced oscillators focused on discrete-time mappings and two-frequency forcing [Glendinning and Wiersig, 1999, Osinga et al., 2000, Belogortsev, 1992, Broer and Simó, 1998]. They uncovered interesting dynamics including Arnol'd or mode-locked tongues consisting of 'interlocking' bubbles and open regions of multistability, nonsmooth bifurcations, and strange nonchaotic attractors. Here, we consider quasiperiodic forcing with 35 frequency components and focus on the regions of mode locking. Our approach is based on instabilities of attracting trajectories in the (x, y, t) phase space of the continuous-time forced system because they relate directly to the concept of generalized synchronization. We can provide a systematic study of generalized synchronization to astronomical forcing by demonstrating existence of such trajectories and exploring their *local* and *global* stability properties. More specifically, we perform three types of calculations. Firstly, a clustering detection

² We give in the Appendix B a summary description of the classical van der Pol oscillator and of its dynamical behaviour.

³ Note that the van der Pol oscillator model is also used as a reference in [Saltzman, 2002, page 101] for a coupled ocean/sea-ice model.

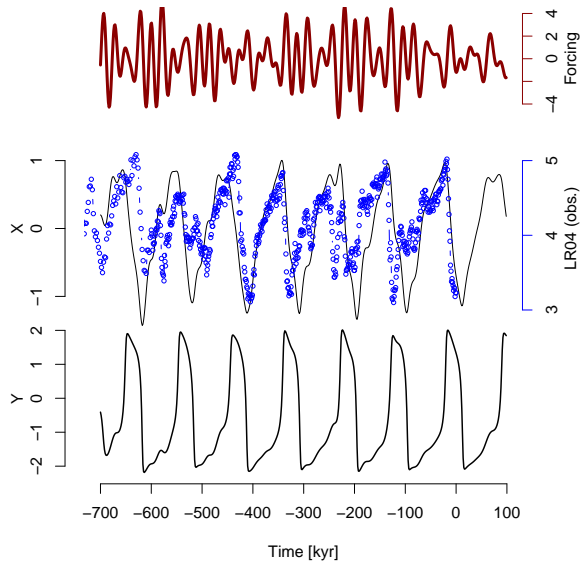


Figure 3: *Top*: the insolation forcing $F(t)$, scaled by a_{ε_1} in order to work dimensionless. *Bottom*: the x and y climatic trajectories obtained using system Eq. (4) with $\alpha = 11.11$, $\beta = 0.25$, $\gamma = 0.75$ and $\tau = 35.09$. With these parameters, $\omega_{\varepsilon_1} = 2.5\omega_{ULC}$, where ω_{ε_1} is the angular velocity associated with the dominant harmonic of obliquity and ω_{ULC} is the angular velocity associated with the unforced system's periodic orbit. Blue dots correspond to the Lisiecki and Raymo stack (LR04) described in Fig. 1(a). Time $t = 0$ corresponds conventionally to the year 1950. The model is in good agreement with the ice volume proxy.

technique uncovers parameter regions with monostable (unique) and multistable (non-unique) synchronization. Secondly, the largest Lyapunov exponent along AT quantifies its long- and short-term local (linear) stability. Thirdly, a basin of attraction of AT quantifies its global (nonlinear) stability. Finally, we remark that in the theory of nonautonomous dynamical systems, attracting trajectories in the (x, y, t) phase space are linked to a modern and more general concept of a *pullback attractor* [Kloeden, 2000, Langa et al., 2002, Kosmidis and Pakdaman, 2003, Wiggins, 2003].

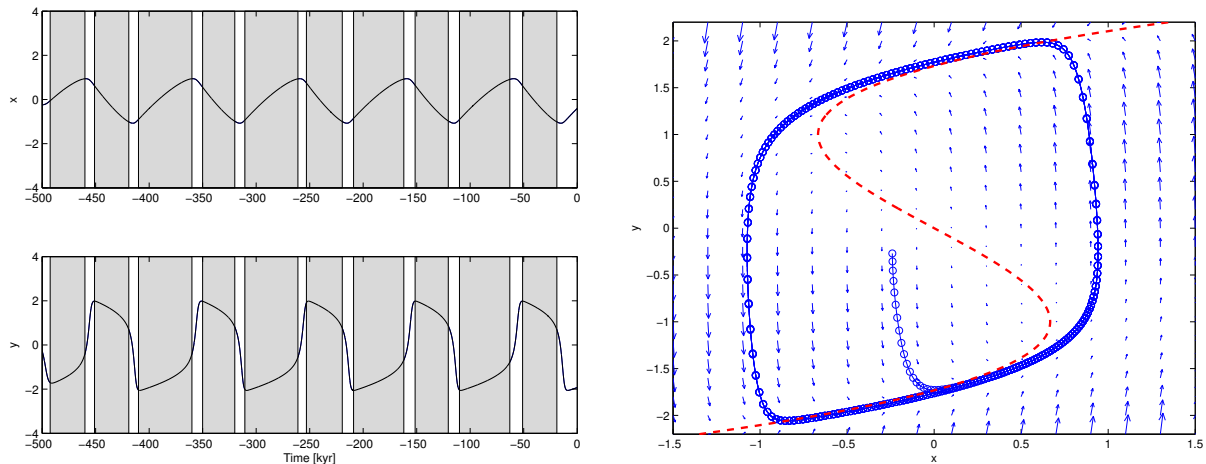
3 Synchronization of the paleoclimatic system to the insolation forcing

Illustration of the synchronization phenomenon

A typical climatic trajectory for $\gamma = 0$ is shown in Fig. 4, from two different points of view: the time series and the phase space portrait. In the time series, we recognize the slow variable x (the ice volume), while y exhibits slow-fast dynamics. This climatic trajectory is also shown in the two-dimensional (x, y) phase space of the autonomous system where arrows indicate direction of the flow. The trajectory converges to the limit cycle with slow-fast dynamics (the speed along the trajectory can be visually assessed by the circles of the residence plot). Let us now consider a set of 70 random initial conditions in the (x, y) -plane at time $t_0 = 0$, and study the resulting climatic trajectories in the three-dimensional phase space (x, y, t) of the nonautonomous system (Fig. 5(a)) for time $t > t_0$. One clearly sees that all trajectories converge to a cylinder—the attracting set in the (x, y, t) space.

However, if we consider now an external forcing ($\gamma > 0$) then *synchronization* onto this forcing may occur under certain conditions [Ashkenazy, 2006, Tziperman et al., 2006]. According to our definition (2–3), synchronization is represented by an attracting climatic trajectory in the (x, y, t) phase space.

Consider first the case of a purely periodic forcing with a period of $T_F = 41$ kyr and strength $\gamma = 3.33$. The 70 initial conditions give rise to climatic trajectories that, after a sufficiently long integration time, converge to two *attracting trajectories* (see Fig. 5(c)). Both attracting trajectories are periodic with period of $T_R = 2T_F = 82$ kyr, and time-shifted versions of each



(a) Time series : x (the ice volume) is the slow variable, while y exhibits slow-fast dynamics. The same color convention white/grey as in Fig. 1 has been used in order to highlight the slow and fast episodes.

(b) Phase space portrait in the two-dimensional (x, y) phase space of the autonomous system: dynamical flow, limit cycle and residence plot (circles are spaced at every 0.5 kyr). More time is spent along the slow manifold (red dashed curve, corresponding to the function $\Phi'(y) = y^3/3 - y = x$). The trajectory converges to the limit cycle (thin curve) with slow-fast dynamics.

Figure 4: Dynamics of the unforced ice ages model Eq. (4) with $\alpha = 11.11$, $\beta = 0.25$, $\gamma = 0$ and $\tau = 35.09$. The slow-fast variable is y , while x is always slow. Example of a typical climatic trajectory with initial conditions $(x_{-500}, y_{-500}) = (-0.24, -0.27)$.

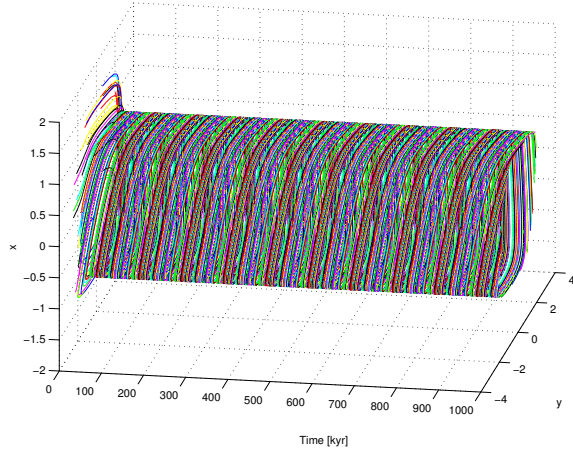
other. This phenomenon is described in the literature as $2:1$ *phase-locking* or *frequency-locking*. Generally speaking a $n:m$ *frequency-locking* is defined as a fixed-in-time relation between the frequencies of the forcing (ω_F) and the oscillator response (ω_R) of the form $n\omega_R = m\omega_F$, where m and n are integers [Pikovsky et al., 2001, p.52].

Then consider the case of the quasiperiodic insolation forcing described in Eq. (1) with $\gamma = 0.75$ and $\tau = 43.86$. Figure 5(e) shows that the 70 climatic trajectories now converge onto three *attracting trajectories*, which reveals that synchronization can be *multistable* [Pikovsky et al., 2001, p.348], [Balanov et al., 2009, p.94]. This phenomenon is described in the literature as *mode-locking* [Svensson and Coombes, 2009]. Note that because of the quasiperiodicity of the insolation forcing, these attracting trajectories are *no longer* periodic nor time-shifted versions of each other. The number of attracting trajectories depends on many factors including the dynamics of the unforced system, the nature of the forcing $F(t)$, and the amplitude γ of the forcing. We will study this in more details in Sec. 4.

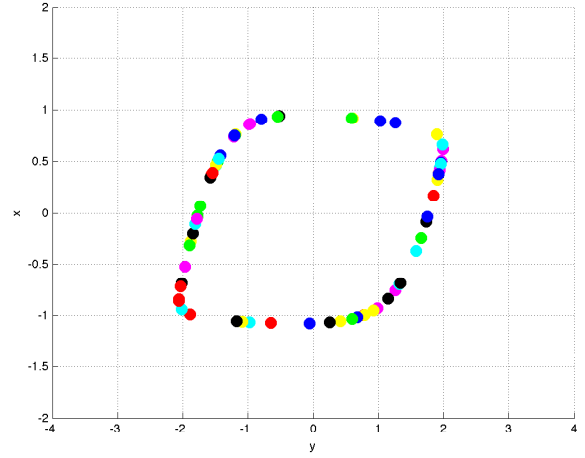
Detection of synchronization by the way of the largest Lyapunov exponent (LLE or λ_{max})

Local or linear stability of an attracting climatic trajectory can be quantified with the largest Lyapunov exponent (LLE) denoted here as λ_{max} [Benettin et al., 1980]. The quantity λ_{max} is a measure of the (average) exponential rate of divergence ($\lambda_{max} > 0$) or convergence ($\lambda_{max} < 0$) of nearby climatic trajectories. Therefore, a negative value of λ_{max} indicates a locally attracting climatic trajectory or *generalized synchronization* [Pikovsky et al., 2001, Wiczeorek, 2009]. A transition from $\lambda_{max} < 0$ to $\lambda_{max} = 0$ indicates a bifurcation where the attracting climatic trajectory disappears and generalized synchronization is lost. Null and positive values of λ_{max} indicate lack of synchrony (positive λ_{max} indicates chaos but this regime is not encountered here). In the case of periodic forcing, computations of λ_{max} can be easily validated with more precise and reliable numerical bifurcation continuation techniques (see § '41 kyr periodic forcing' below).

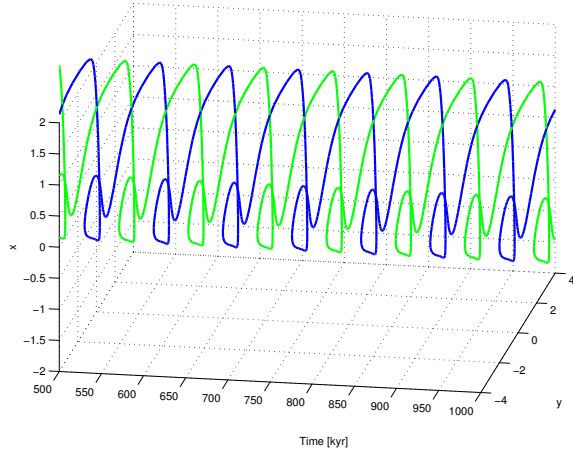
Long-term λ_{max} and short-term λ_{max}^H LLE's



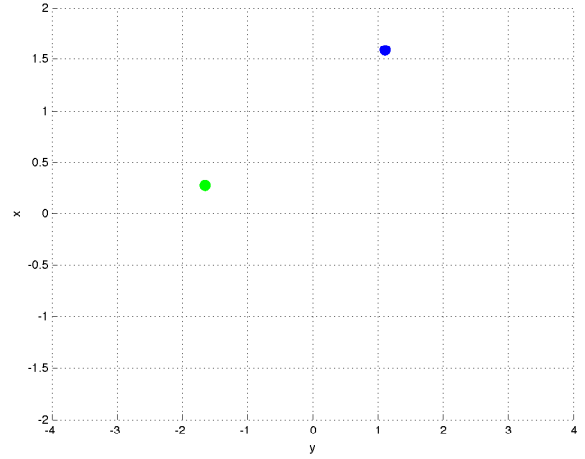
(a) without any forcing ($\gamma = 0$, $\tau = 35.09 \rightarrow T_{ULC} \approx 100$ kyr): all trajectories converge to a cylinder—the attracting set in the (x, y, t) space.



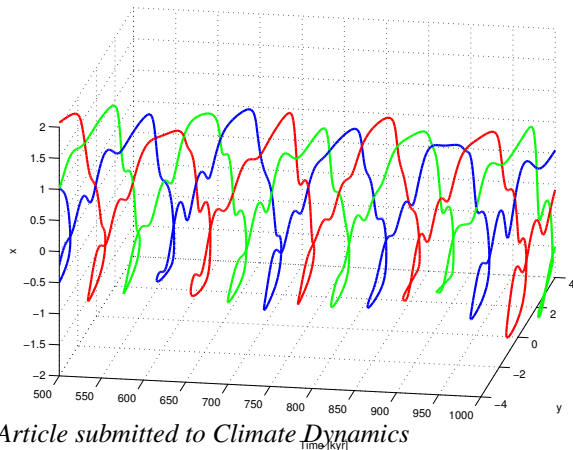
(b) Section of Fig. 5(a) at $t = 550$ kyr: no clear dense cluster of climatic trajectories is identified: no attracting trajectory does exist.



(c) with a purely periodic forcing with a period of $T_F = 41$ kyr ($\gamma = 3.33$, $\tau = 35.09 \rightarrow T_{ULC} \approx 100$ kyr): the trajectories converge to two attracting trajectories of period 82 kyr: there is a frequency-locking 2:1.

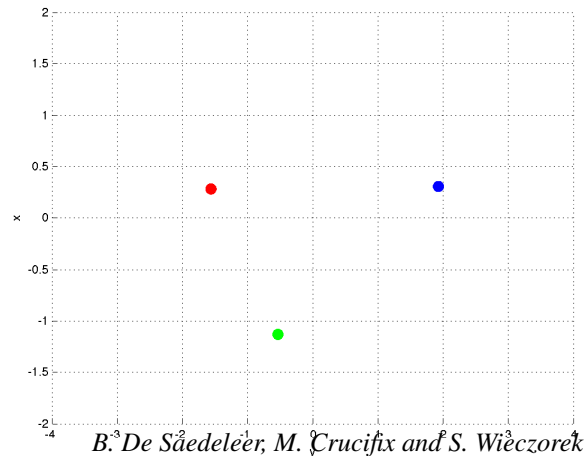


(d) Section of Fig. 5(c) at $t = 550$ kyr: two clusters are identified, corresponding to the two attracting trajectories born from frequency-locking 2:1.



Article submitted to *Climate Dynamics*

(e) with the quasiperiodic insolation ($\gamma = 0.75$, $\tau = 43.86 \rightarrow T_{ULC} \approx 125$ kyr) given by Eq. (1): the trajectories converge now to three attracting trajectories for a long time, revealing a multistable synchronization.



(f) Section of Fig. 5(e) at $t = 550$ kyr: three clusters of trajectories are identified, corresponding to the three attracting trajectories born from multistable synchronization.

Figure 5: Illustration of three different paleoclimate dynamical regimes: (top) without any forcing, (middle) frequency-locking 2:1 onto a 41 kyr periodic forcing (symbol '+' in Figs. 6(a) and 6(c)), (bottom) generalized multistable synchronization on the quasiperiodic insolation forcing (symbol 'x' in Figs. 6(b) and 6(d)). The ice

The largest Lyapunov exponent λ_{max} is mathematically defined⁴ as [Ott, 2002] :

$$\lambda_{max} = \lim_{|\delta \mathbf{Z}(0)| \rightarrow 0} \lim_{t \rightarrow \infty} \frac{1}{t} \ln \frac{|\delta \mathbf{Z}(t)|}{|\delta \mathbf{Z}(0)|} \quad (5)$$

where $\delta \mathbf{Z} = [\delta x, \delta y]$ are vanishing perturbations about x and y , respectively, governed by the linearization of system Eq. (4). Whereas this classical λ_{max} is defined in long term limit ($t \rightarrow \infty$), one can also define [Abarbanel et al., 1991] a *short-term* version, λ_{max}^H , by considering a finite time interval H ($H = 50$ kyr will be considered in this article):

$$\lambda_{max}^H = \lim_{|\delta \mathbf{Z}(0)| \rightarrow 0} \frac{1}{H} \ln \frac{|\delta \mathbf{Z}(H)|}{|\delta \mathbf{Z}(0)|} \quad (6)$$

While λ_{max} gives the average or long-term stability information, λ_{max}^H can tell us about the behaviour of nearby trajectories within a short time interval H . For example, $\lambda_{max} < 0$ does not necessarily imply $\lambda_{max}^H < 0$ for some suitably chosen H . The definition (6) will be useful in studying the robustness of generalized synchronization in Sec. 6.

For computing λ_{max} , as the system Eq. (4) and the Jacobian have an analytical form, tangent space methods [Kantz and Schreiber, 2004] can be used; technical details are given in the Appendix C.

Influence of the parameters γ and T_{ULC}

The two particular types of synchronization illustrated in Fig. 5(c) and 5(e) have been obtained for a fixed value of the amplitude γ of the external forcing and of the natural period of the unforced paleoclimatic system T_{ULC} . Now, we are equipped to achieve a much broader view of the dynamics by performing a parametric study on these two parameters. The quantity plotted in Figs. 6(a) and 6(b) is the largest Lyapunov Exponent at 3 Myr, far from the transient behaviour so that $\lambda_{max}^{H=3 \text{ Myr}}$ may already been considered as a good approximation of λ_{max} .

41 kyr periodic forcing

⁴Even if differential versions of the LLE have sometimes been developed mainly for computational efficiency purposes, we however preferred within this article to stick on the original definition of the LLE, because it is more standard and there is no insistent need for lowering computation time in the present framework, as the number of degrees of freedom of the system is reduced.

Fig. 6(a) corresponds to the case of the 41 kyr periodic forcing ($T_F = 41$ kyr). The synchronization region ($\lambda_{max} < 0$) is composed of several V-shape regions, called *Arnol'd tongues* (phase- or frequency-locking), originating at 1, 2, 3, etc. times the forcing period T_F . These regions correspond to 1:1, 2:1, 3:1 frequency-locking zones (3:2 and 5:2 can also be guessed). Periodic solutions are found within these regions which originate generally speaking at $T_{ULC} = (m/n) T_F$. No synchronization is possible when γ is zero but synchronization may occur already for infinitesimally small γ . Then, for increasing γ , the synchronization region widens and synchronization becomes more stable up to an optimum value γ^* of the forcing. When $\gamma > \gamma^*$, the synchronization becomes less and less effective, because at large γ the system is too much steered away from its natural dynamics; it may even be driven into chaos at yet higher forcing amplitude [Metin et al., 1993] but this case is beyond our focus.

In order to perform an accurate validation of the synchronization region given by the LLE ($\lambda_{max} < 0$) method, we computed the main Arnol'd tongues boundaries with the more accurate numerical continuation methods such as AUTO [Doedel et al., 2009]. The case of periodic forcing [$F(t) = \sin(\omega t)$] with $\beta = 0$ has been already extensively studied in the literature, analytically assuming some approximations [Guckenheimer and Holmes, 1983, p.70–75], and using numerical algorithms for pseudo-arc length continuation [Metin et al., 1993]. The usual approach extends the original nonautonomous system by additional differential equations for the forcing so that the system becomes autonomous, and then explores the (ω, γ) parameter space. Note that the asymmetry introduced here with the parameter β adds slightly more complexity and induces additional features to the diagrams documented in these papers. In this way, we computed Arnol'd tongue boundaries as saddle-node of limit cycle bifurcations for the extended system with $\alpha = 11.11$ and $\beta = 0.25$.

Superposition of LLE calculations and bifurcation boundaries in Fig. 6(a) shows that the synchronization regions obtained with two different techniques match perfectly. This is a confirmation that the method based on the LLE works fine and we will be able to use it for the case of the quasiperiodic insolation forcing. Note that bifurcation boundaries are also drawn in Fig. 6(c) in order to stress the correspondence with yet another method of detecting synchronization that will be discussed in Sec. 4.

Astronomical quasiperiodic forcing

For the case of the quasiperiodic insolation forcing (Fig. 6(b)), the region of synchronization appears to be in one single piece with some indications of well-separated tongues (mode locking) at small γ . In other words, whatever the value of the natural period T_{ULC} of the paleoclimatic system, it has a higher probability of being synchronized onto the insolation forcing. Of course, for very low values of γ , there is still no synchronization. Note that γ has been downscaled by $\sigma_{insol} \approx 5$ (compared to $\sigma_{sine} = \sqrt{2}/2$ for the 41 kyr periodic forcing), in order to keep a realistic range comparison.

4 Non uniqueness: multistability and basins of attraction

The detection of synchronization using the LLE ($\lambda_{max} < 0$) gives only an Yes/No-type of information, without making any distinction between different tongues as this would require information about multistability. For example, Fig. 6(b) indicates synchronization for the parameter settings marked with the symbol 'x' but gives no information about the number of attracting trajectories (we know that there are three different attracting trajectories from Fig. 5(e)). To explore the problem of multistable synchronization, we propose a *clustering method* that not only allows us to detect synchronization, but additionally provides information about the *number of attracting trajectories* denoted here with N .

Multistability Analysis: numerical estimate of the number of attracting trajectories N by a clustering technique

Consider the case of the quasiperiodic insolation forcing with the three attracting trajectories, i.e., $N = 3$ (Fig. 5(e)). Although N can often be easily assessed visually, we want to automatically detect and count the number of ATs. As a matter of fact, N can be easily estimated in the following way. Fix a time t that defines a two-dimensional (x, y) -section in the (x, y, t) phase space. Then start with a grid of initial conditions at some time $t_0 < t$ and take $t - t_0$ sufficiently large so that all the initial conditions converge to the attracting trajectories at t . Since each AT is represented by a point on the (x, y) -section, the problem of counting attract-

ing trajectories reduces to a simple clustering problem. We designed a suitable automatic cluster detection algorithm that counts the number of clusters to obtain an estimate of N . For example, Fig. 5(f) shows⁵ the (x, y) -section of the three-dimensional (x, y, t) phase space at $t = 550$ kyr, given 70 initial conditions at $t_0 = 0$. The 70 trajectories converge onto three (highly concentrated) clusters corresponding to the three attracting trajectories.

The idea of using clustering analysis for paleoclimatic dynamics comes from the natural fact that clustering is another way of looking at generalized synchronization where negative LLE makes the trajectories cluster more efficiently. This provides another insightful viewpoint on the problem of identification of number of synchronized solutions of the paleoclimatic system: the more stable the synchronization, the more efficient formation of clusters.

Two important aspects of cluster analysis⁶ have to be considered to avoid risks of mis-identification of clusters:

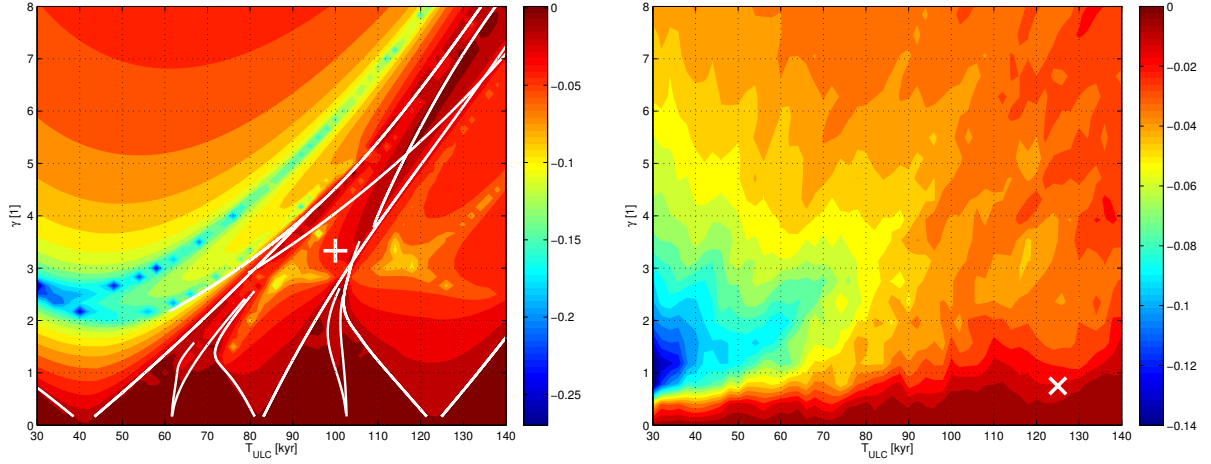
- the notion of a cluster is based on the *threshold distance* d_T ⁷ that has to be carefully chosen. If d_T is chosen too large, there will be just one cluster including all points; if it is too small, no clusters will form with more than one point.
- in order to have sufficiently well formed clusters, the time interval $t - t_0$ must be chosen large enough so that the transient behaviour is gone; an illustration of the convergence is given in Fig. 7.

Depending on the type and amplitude of the forcing γ , we can have potentially a whole range of possible number of attracting trajectories N , ranging from *one* [Tziperman et al., 2006], to *a few* (two in the 41 kyr periodic forcing example in Figs. 5(c) and 5(d), or three in the quasiperiodic insolation forcing example in Figs. 5(e) and 5(f)). When no forcing is considered

⁵See also Fig. 18 for a detailed view.

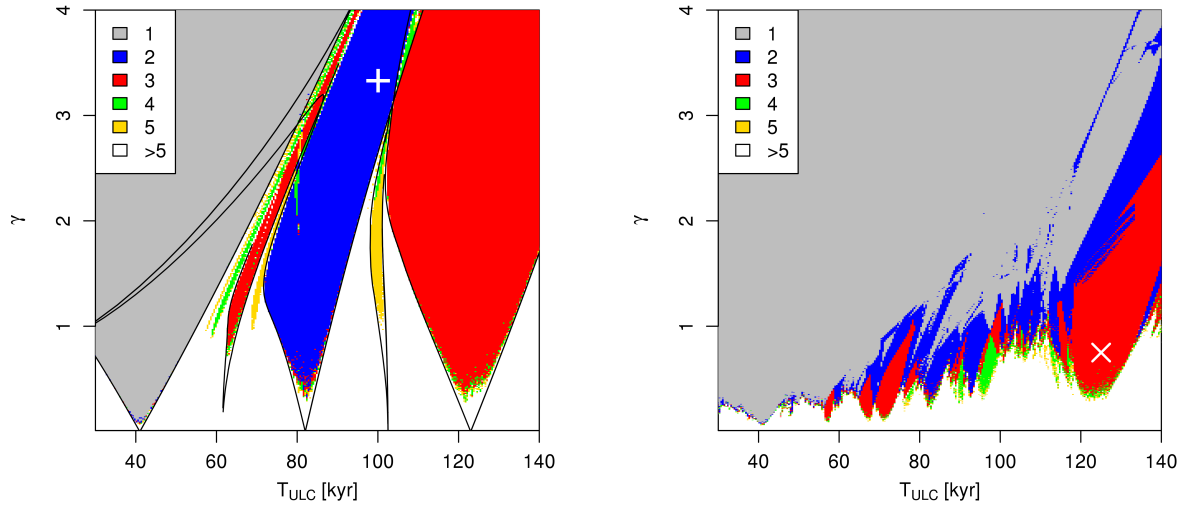
⁶Cluster analysis or *clustering* is the assignment of a set of observations into subsets (called clusters) so that observations in the same cluster are similar *in some sense*. This is a common technique for statistical data analysis used in many fields for countless applications. There exists many types of clustering, along with several methods, among which: hierarchical, partitional, spectral, kernel PCA (principal component analysis), k-means, c-means and QT clustering algorithms.

⁷This threshold distance d_T appears in any computation related to clustering analysis, or analogically Recurrence Plots (RP) analysis in complex networks, for determining neighbours [Marwan et al., 2009, Donges et al., 2009].



(a) Largest Lyapunov Exponent λ_{max} [kyr^{-1}] for the 41 kyr periodic forcing case. The region with $\lambda_{max} < 0$ corresponds to synchronization; we recognize its underlying Arnol'd tongue structure. The bifurcation boundaries of the Arnol'd tongues obtained with the more accurate numerical continuation method AUTO are superimposed, for validation purposes (white curve), and match perfectly.

(b) Largest Lyapunov Exponent λ_{max} [kyr^{-1}] in the case of the quasiperiodic insolation forcing given by Eq. (1): the broad region of synchronization is a typical signature of the quasiperiodic insolation. The region of synchronization appears to be in one single piece with some indications of well-separated tongues (mode locking) at small γ .



(c) Numerical estimate of the number of attracting trajectories N for the 41 kyr periodic forcing case. In practice, small positive values correspond to synchronization onto a few attracting trajectories, while high values indicate no synchronization. Now the region inside the synchronization tongues is colored in function of N . For the tongue corresponding to a frequency-locking $n : 1$, we have n attracting trajectories. The bifurcation boundaries of the Arnol'd tongues obtained with the more accurate numerical continuation method AUTO are superimposed, for validation purposes (black curve), and match perfectly.

(d) Numerical estimate of the number of attracting trajectories N in the case of the quasiperiodic insolation forcing given by Eq. (1): the structure is now much more complex, consisting of intermingled series of Arnol'd tongues. The region with one attracting trajectory, corresponding to *unique or monostable generalized synchronization*, is the largest. However, there are also parameter sets with $N = 2, 3$ or even more attracting trajectories.

Figure 6: Detection of synchronization by two different methods: the largest Lyapunov Exponent ($\lambda_{max} < 0$) (top) and the numerical estimate of the number of attracting trajectories N by a clustering technique (bottom), and for two different types of forcing: a 41 kyr purely periodic forcing (left) and the quasiperiodic insolation forcing given by Eq. (1) (right). These diagrams show for which values of the parameters $\{T_{ULC}, \gamma\}$ synchronization of the climate system occurs for the ice age model Eq. (4) with $\alpha = 11.11$, $\beta = 0.25$, and $\tau = 35.09$. The symbol (+) refers to the specific climatic attracting trajectories illustrated in Fig. 5(c) in the 41 kyr periodic forcing case, for which $N = 2$. The symbol (x) refers to the specific climatic attracting trajectories illustrated in Fig. 5(e) in the quasiperiodic insolation forcing case, for which $N = 3$.

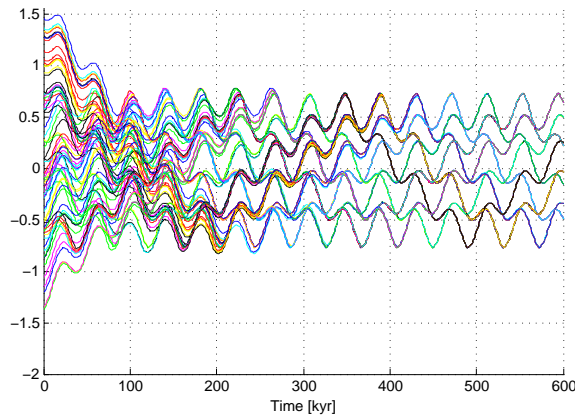


Figure 7: Illustration of the importance of choosing the time interval $t - t_0$ large enough so that the transient behaviour is gone, in order to have sufficiently well formed clusters. Here, choosing $t = 550$ kyr ensures that the eight clusters are already formed, starting from $t_0 = 0$.

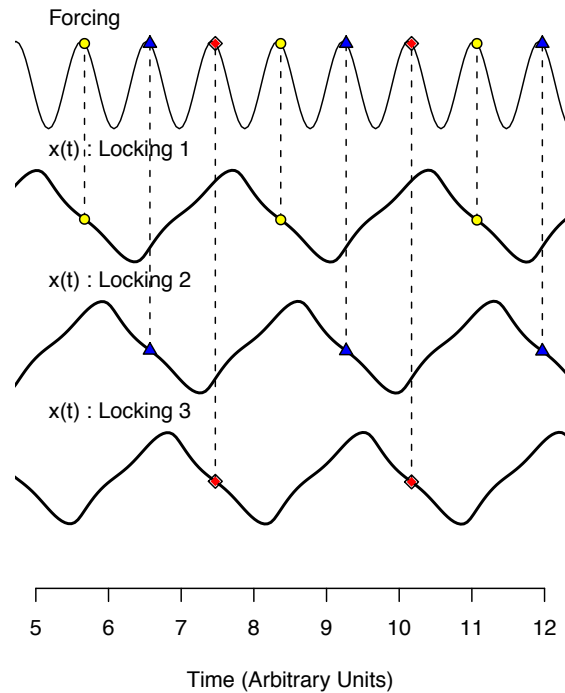


Figure 8: Illustration of the three possible synchronized solutions ($N = 3$) existing for the frequency-locking 3:1 on a purely periodic forcing, in the time series format. The response can be locked on one of the periods of the forcing.

(Figs. 5(a) and 5(b)), or there is forcing but no synchronization occurs, we find no clusters at all. This means that there are as many points in the (x, y) -section at time t as initial conditions at time t_0 . Clearly, it is difficult to numerically distinguish between no synchronization and a large number of attracting trajectories ($N \gg 1$). Therefore, we restrict ourselves to just six different regions in Fig. 6, where we use white to indicate when there are none or more than five attracting trajectories.

Now, we apply the numerical clustering analysis in the case of the periodic forcing (Fig. 6(c)) and of the quasiperiodic forcing (Fig. 6(d)). We set $t = 0$ and consider a grid of 49 initial conditions covering $x \in [-2.2; 2.2]$ and $y \in [-2.2; 2.2]$ at the initial time $t_0 = -40T_F$ for the periodic forcing (T_F is the period of the forcing), and $t_0 = -1600$ kyr for the astronomical forcing. Two points in the (x, y) -section are estimated to belong to a different cluster if their Euclidean distance is greater than 0.1.

41 kyr periodic forcing

An illustration of the three possible synchronized solutions ($N = 3$) existing for the 3:1 frequency-locking on a periodic forcing is given in Fig. 8, where the response can be locked on one of the periods of the forcing. More generally, N corresponds to the num-

ber of forcing cycles associated with the synchronization regime ($N = 1$ for 1:1; $N = 2$ for 2:1; $N = 3$ for 3:2, 3:1, etc.)⁸. The resulting pattern of different N is, as expected, in agreement with the bifurcation diagram (Fig. 6(c)). For example, $N = 3$ in the 3:1 tongue. This method allows one to visualize the 4:3 ($N = 4$) and even the 5:4 ($N = 5$) tongues to the left of the 3:2 tongue. It is also seen that N is generally larger where different synchronization regimes co-exist; this is the case between the 2:1 and 3:1 regimes around $\gamma = 4$.

Astronomical quasiperiodic forcing

Fig. 6(d) shows that synchronization occurs for most parameter configurations. The region with one attracting trajectory ($N = 1$), corresponding to

⁸This statement relies on the system invariance with respect to a time-shift of one forcing period ([Tziperman et al., 2006] show a very nice illustration of this point).

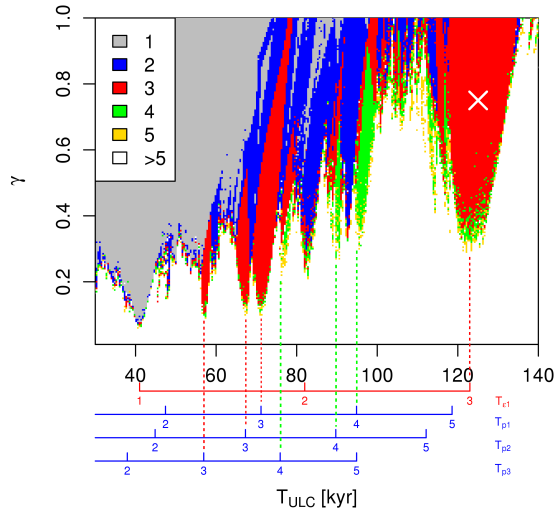


Figure 9: A careful examination of the lower part (low γ) of Fig. 6(d) allows an insightful physical interpretation. The underlying structure of the intermingled series of Arnol'd tongues can be understood: it is a mixing of several Arnol'd tongues series corresponding to each of the main components of the spectrum of the astronomical forcing, yielding a resulting pattern which looks like misaligned combs. Subscales based on the period of the four main components (ϵ_1 , p_1 , p_2 and p_3) of the insolation highlighted in Fig. 2 allows a clear recognition of each individual Arnol'd tongues series.

unique or monostable generalized synchronization [Rulkov et al., 1995], is the largest. However, there are also parameter sets with $N = 2, 3$ or even more attracting trajectories. They indicate *multistable generalized synchronization* where different possible stable relationships (2) between the forcing and the oscillator response coexist.

A closer view in the lower values of γ is given in Fig. 9, which allows an insightful physical interpretation.

Three tongues with $N = 1, 2, 3$ are rooted at $T_{ULC}/T_{\epsilon_1} = 1, 2$ and 3 , respectively, suggesting a synchronization on the main obliquity component of the astronomical forcing of the same nature as synchronization on a periodic forcing. A series of other synchronization tongues with $N > 1$ appear; they correspond to 2:1 ($N = 2$), 3:1 ($N = 3$), 4:1 ($N = 4$) and even 5:1 ($N = 5$) synchro-

nization on the three leading components of precession, denoted p_1 , p_2 and p_3 . Consequently, the richness of the astronomical forcing effectively widens the parameter range for which synchronization occurs, compared to a periodic forcing. The phenomenon may be understood intuitively: just as you are more likely to tune on some radio station if you are surrounded by a dozen of free FM emitters, the system is more likely to synchronize on the rich astronomical forcing than on a periodic forcing. Synchronization with $N = 1$ or 2, found for larger γ , can be interpreted as a form of combined synchronization on both obliquity and precession.

It is crucial to appreciate that synchronized solutions are not periodic and that, unlike the periodic forcing case, different synchronized solutions for a given set of parameters are not time-shifted versions of each other. The idea that different synchronized solutions coexist is of practical relevance for paleoclimate theory. Namely, the set of parameters used to obtain the fit to the paleoclimatic records shown in Fig. 3 give two distinct solutions at $t = 0$ when started from a grid of initial conditions at $t_0 = -700$ kyr. Sensitivity studies show that the choice of $t - t_0$ is sometimes important for estimating correctly N . However, tests with $t - t_0$ as large as 200 Myr of astronomical time suggest that several attracting trajectories may co-exist at the asymptotic limit of $t_0 \rightarrow -\infty$.

A similar numerical clustering analysis plot for $\beta = 0.6$ is shown in Fig. 10 in order to give an idea of the effect of this parameter (a more detailed analysis is performed in Sect. 5). The main conclusion about the multistability remains, but the particular values of N change, as the intermingled tongue series are different.

Evolving shape of the basins of attraction

Each AT_i ($i = 1 \dots N$) has its own *basin of attraction*⁹ [Barnes and Grimshaw, 1997], that is defined as the set of all initial conditions in the (x, y, t) phase space that converge to that AT_i as time tends to infinity. For our nonautonomous system Eq. (4), we can study basins of attraction in the (x, y) -section for different but fixed values of initial time t_0 , and observe how they vary with t_0 . A given initial condition at time t_0 lies in the basin of attraction of AT_i if it approaches AT_i as time tends to infinity. Technical details about the computation of the

⁹ A more formal definition of the *basin of attraction* for nonautonomous dynamical systems is given in [Kloeden, 2000, Langa et al., 2002].

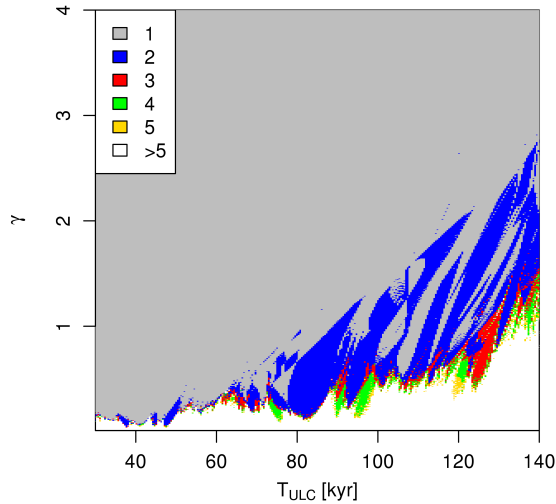


Figure 10: Same as Fig. 6(d), but now with $\beta = 0.6$ instead of $\beta = 0.25$. The particular values of N change, as the pattern of intermingled tongue series is different, but the main conclusion about the multistability remains.

basins of attraction by use of the specific classification algorithm developed (see Fig. 18) are given in the Appendix D. Basins of attraction are of major importance because they provide the information about global or nonlinear stability of synchronization. If we care about predictability, basin boundaries indicate when a change in the attracting climatic history is likely.

The evolving shape of the basins of attraction is shown in Figs. 11 and 12, for the case of 41 kyr periodic forcing and the quasiperiodic astronomical forcing, respectively. The evolution is shown as a comic strip, where each subfigure has an x -axis ranging from -1.5 to 1.5, and a y -axis ranging from -2.5 to 2.5 (the axis labels have been removed for a better readability).

In the case of a periodic forcing (two basins), the pattern repeats itself periodically (compare the $t_0 = 0$ kyr to $t_0 = 40$ kyr, and to $t_0 = 80$ kyr subfigures) in Fig. 11. However, in the case of the quasiperiodic forcing (three basins), the pattern is much more intricate and seems not to repeat itself for the time horizon considered here.

The ratio between the area of a basin of attraction and the considered area of the phase space can be interpreted as a probability to converge to the corresponding attracting trajectory when starting from a randomly

chosen initial condition. In the case of the periodic forcing, the two ATs are roughly equally likely for all t_0 as could be guessed from Fig. 5(c). However, this is not the case for the quasiperiodic forcing where the probability to reach the same attracting trajectory may vary significantly in time. For example, the yellow basin is rather small at $t_0 = 0$ kyr but becomes much larger at a later time $t_0 = 90$ kyr.

In the multistable regime, if an AT_i happens to lie sufficiently close to its basin boundary, then small perturbations could make the climate jump to another (coexisting) $AT_{j \neq i}$, reducing predictability. This phenomenon is illustrated in Sec. 6.

5 Influence of the symmetry-breaking parameter β

As the parameter β controls the asymmetry of the glaciation/deglaciation saw-tooth structure (a higher value of β leads to an enhanced asymmetry), it is useful to investigate its effect. We have already indicated in Fig. 10 that multistability depends on β in the case of the quasiperiodic insolation forcing. A more systematic approach encompassing the whole range of β is shown in Figs. 13(a) and 13(b), for the case of 41 kyr periodic forcing and the quasiperiodic astronomical forcing case, respectively.

First consider the 41 kyr periodic forcing (Fig. 13(a)). To understand this Figure, recall that the unforced oscillator (i.e., $\gamma = 0$) has a stable fixed point for $|\beta| > 1$ and a stable limit cycle for $|\beta| < 1$.

The system responds almost *linearly* to the forcing when $|\beta|$ is sufficiently large. This explains regions of unique synchronization ($N = 1$) where only one climate response is possible. The system becomes *excitable* when $|\beta|$ is just slightly greater than one. If the forcing is large enough it will excite oscillations. In this case, N is equal to the number of initial conditions if synchronization is lost, or to a smaller number if synchronization occurs.

Consider now the interval $-1 < \beta < 1$. For this, keep in mind (i) that the period of the unforced oscillation varies by almost a factor of two within the range $0 < |\beta| < 1$, and (ii) that synchronization requires some relation between the period of the unforced oscillations and the forcing period. Consequently, synchronization on the periodic forcing occurs only for fairly narrow ranges of β that are symmetric around zero. The fig-

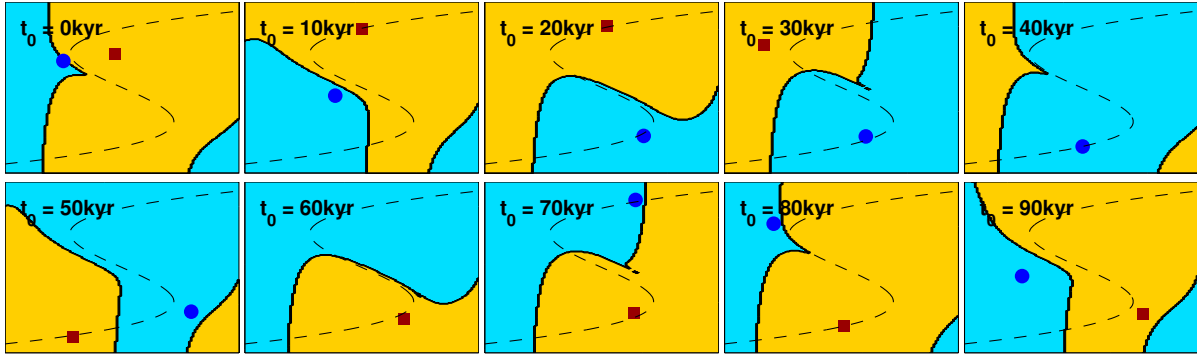


Figure 11: Evolving shape of the two basins of attraction for system Eq. (4), with $\alpha = 11.11$, $\beta = 0.25$, $\gamma = 3.33$ and $\tau = 35.09$. Case of a 41 kyr periodic forcing : the pattern is 82 kyr periodic (frequency-locking 2:1). The function $\Phi'(y) = y^3/3 - y = x$, corresponding to the slow manifold, is also shown (dashed curve). The attracting trajectories (symbol) sometimes lie close to the boundary of their own basin of attraction.

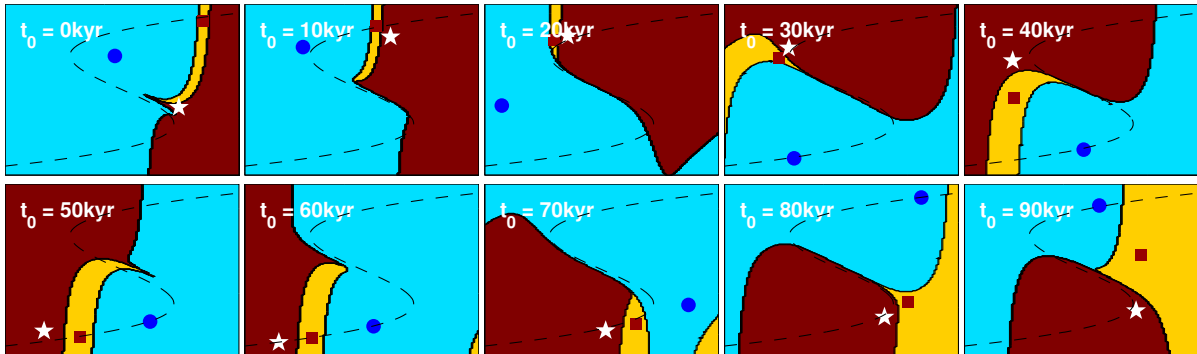


Figure 12: Evolving shape of the three basins of attraction for system Eq. (4), with $\alpha = 11.11$, $\beta = 0.25$, $\gamma = 0.12$ and $\tau = 35.09$. Case of the quasiperiodic insolation given by Eq. (1): the pattern is quasiperiodic, constituting the specific signature of the insolation. The function $\Phi'(y) = y^3/3 - y = x$, corresponding to the slow manifold, is also shown (dashed curve). The attracting trajectories (symbol) sometimes lie close to the boundary of their own basin of attraction.

ure reminds us of Arnol'd tongues. The main synchronization regimes detected here correspond to 4:1, 3:1 and 5:2 frequency-locking. Outside these synchronization regimes, the system fails to converge to a sufficiently small set of attracting trajectories, meaning that the forcing is not as an efficient pacemaker.

Finally, compare this situation with that obtained with the astronomical forcing (Fig. 13(b)). Synchronization now occurs in a larger area of the parameter space. Whereas the structure of the periodic forcing is preserved as long as the forcing amplitude is low enough, there is a much more richer and complex pattern of different N for larger γ . This pattern emerges from the interaction with different harmonics and their beatnotes.

6 Robustness of synchronization

Robustness or *reliability* of synchronization can be studied in terms of two properties of an attracting climatic trajectory. Local stability analysis based on the short-term LLE (λ_{max}^H) provides information about the short-term local convergence towards the AT. For example, a temporary loss of local stability indicated by $\lambda_{max}^H > 0$ will cause a temporary loss of synchrony and divergence from the AT even though the trajectory is stable on average ($\lambda_{max} < 0$). Global stability analysis based on the geometry of basins of attraction for different AT's provides information about the system response to external perturbations such as random fluctuations. For example, an external perturbation may push a climatic trajectory outside of the basin of attraction of the AT. Robustness and uniqueness of synchronization are closely linked in the sense that the global stability is a factor only when there are coexisting attracting trajectories. Robustness is compromised most when a temporary loss of local stability coalesces with a weakening of the global stability. We will now briefly discuss these two effects that could restrict the prediction horizon for the evolution of climatic trajectories.

Temporary desynchronization via loss of local stability

Some additional experiments made in our paleoclimatic framework reveal another strange behaviour in the system Eq. (4), that can be deduced from a careful inspection of Fig. 14. In the presence of small additive noise, we notice that nearby trajectories could diverge

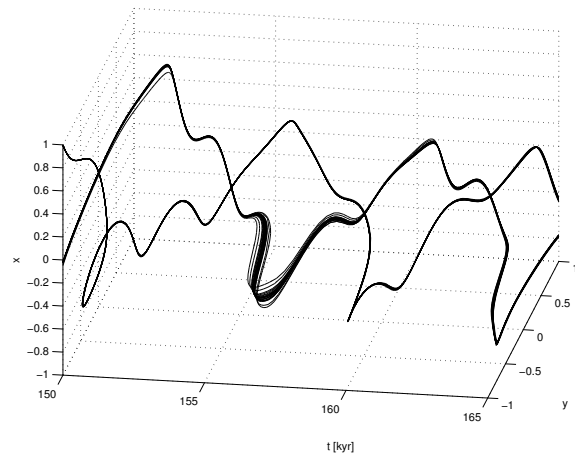


Figure 14: The temporary divergence of nearby climatic trajectories reveals short-term local instabilities (e.g. around $t \approx 157$ kyr). This illustration was obtained by considering a set of 50 random initial conditions at $t_0 = 0$ within $x \times y \in [-1, 1] \times [-1, 1]$, and by adding some noise of small amplitude in the system at every time step in order to trigger the instabilities. The model used is Eq. (4) with $\alpha = 11.11$, $\beta = 0.25$, $\gamma = 0.033$, and $\tau = 33.33$.

for some time, like those around $t \approx 157$ kyr.

Such temporary divergence is similar to desynchronization bursts [Rulkov et al., 1995] and strongly suggests to investigate the evolving sign of the short-term LLE λ_{max}^H along the attracting climatic trajectory. We computed $\lambda_{max}^{H=50 \text{ kyr}}$ along one of the two attracting trajectories of system Eq. (4), subject to insolation forcing given by Eq. (1). The result is shown in Fig. 15, where the attracting climatic trajectory has been coloured according to the values of $\lambda_{max}^{H=50 \text{ kyr}}$. Although the system is synchronized on a long term ($\lambda_{max} = -0.2 \text{ kyr}^{-1}$, see Fig. 17), we see here that there exist episodes with positive values of the short-term¹⁰ LLE λ_{max}^H , revealing temporary desynchronizations [Wieczorek, 2009]. This explains the divergence of nearby trajectories found in Fig. 14.

These results remained unchanged with respect to the most important parameters of the model. For example, our main conclusions about the stability re-

¹⁰ For completeness, the very short-term (*instantaneous*) stability has also been investigated (see Fig. 20 in the Appendix E), as a limit case $H \rightarrow 0$, but it is less physically relevant within the paleoclimatic context.

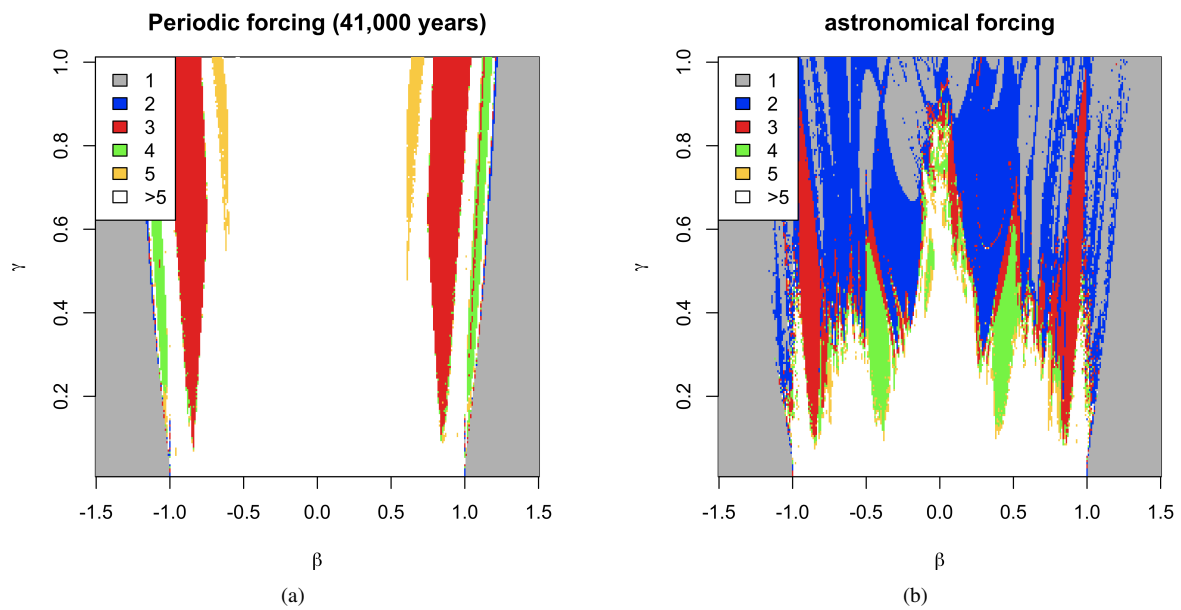


Figure 13: Numerical estimate of the number of attracting trajectories N plotted as a function of the asymmetry parameter β and the amplitude of the forcing γ for the ice age model Eq. (4) with $\alpha = 11.11$, $\beta = 0.25$, and $\tau = 35.09$, assuming (left) a 41 kyr periodic forcing and (right) the quasiperiodic astronomical forcing given by Eq. (1). Synchronization occurs in a larger area of the parameter space in response to the astronomical forcing than in response to the periodic forcing, and the pattern of different N for larger γ is much more richer and complex; this structure emerges from the interaction with different harmonics of the astronomical spectrum and their beatnotes.

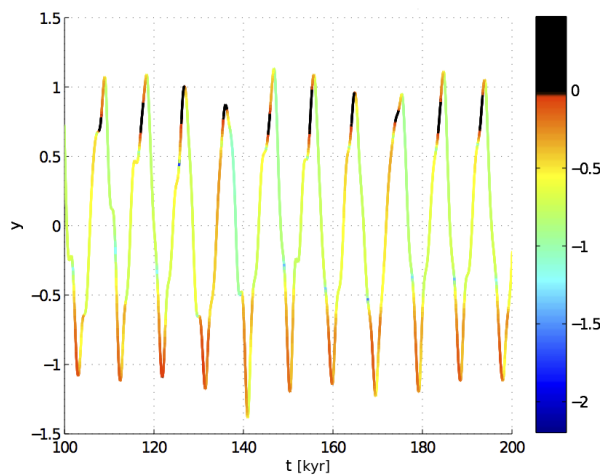


Figure 15: Short-term largest Lyapunov Exponent $\lambda_{max}^{H=50 \text{ kyr}}$ of one of the two attracting trajectories of system Eq. (4), subject to insolation forcing given by Eq. (1), and for the same parameters as in Fig. 14. The attracting climatic trajectory has been coloured according to the values of $\lambda_{max}^{H=50 \text{ kyr}}$, revealing temporary desynchronizations; this explains the divergence of nearby trajectories found in Fig. 14, e.g. around $t \approx 157$ kyr.

main qualitatively valid, even for different values of α (like $\alpha = 100$), or with a different type of potential ($\Phi'_5(y) = (y + 1.7)(y + 1.58)(y + 0.8)(y - 0.5)$), even if the shape and size of the limit cycle and the boundaries of the basins of attraction are of course different. The effect of the insolation function $F(t)$ has also been checked: we compared the attracting trajectories for the insolation given by Eq. (1), compared to those for the insolation given by [Laskar et al., 2004]. As these insolation functions are very similar, the results are also very similar, and no difference was noticed.

At first glance, it may appear that these episodes of temporary divergence are not relevant to the robustness of synchronization because climatic trajectories converge back to the attracting trajectory on a long term. However, other effects may be present that could strongly amplify such temporary divergence. They are identified below.

Sensitivity to perturbations: preliminary results

Consider again Fig. 12 showing (x, y) -sections with coexisting attracting trajectories in the case of the quasiperiodic insolation, and their basins of attraction for different values of t_0 . Suppose now that the system is subject to additive fluctuations (for example, these may represent volcanic eruptions). Under certain conditions, such external perturbations may cause a displacement of the trajectory to a different basin of attraction, causing a jump¹¹ to another attracting trajectory.

As a further illustration of this idea we show in Fig. 16 two attracting trajectories (in the time series format) that coexist for the same system parameters as those used for the fit of Fig. 3, but with additive fluctuations added to the fast variable (see legend for details). A jump from one trajectory to another at around -475 kyr (arrow) may clearly be identified. This shows that a climatic trajectory is robust against fluctuations if it stays away from the basin boundary but its robustness can weaken significantly due to the weakening of the global stability near the basin boundary.

We conclude that externally triggered jumps between coexisting attracting climatic trajectories seem to be most likely when the temporary desynchronization due to the loss of local stability coalesces with the weakening of the global stability due to the proximity to the basin boundary.

¹¹ In the periodic forcing case the phenomenon of jumping from one attracting trajectory to another in response to a perturbation is called a *phase slip* [Pikovsky et al., 2001, p.238].

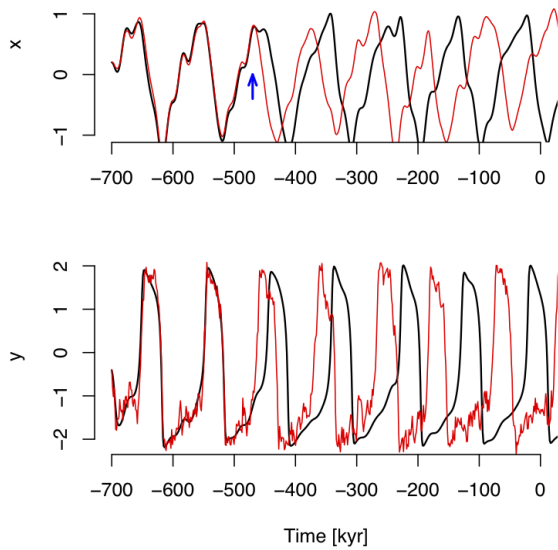


Figure 16: Sensitivity of the climatic system to perturbations. The same solution of the ice ages model Eq. (4) as in Fig. 3 is plotted (black) along with one sample trajectory of the same system (red), but with additive fluctuations added to the fast variable: $dy = -\tau^{-1}(\alpha(\Phi'(y) - x))dt + b dW$, with $b = 0.5\sqrt{\omega_{\epsilon_1}}$ and W a Wiener-process. The arrow shows the time of the jumping from one to the other climatic attracting trajectory, which reduces the predictability of the timing of the glaciations.

7 Conclusions

We have identified, illustrated, and provided a systematic study of *generalized and multistable synchronization* between the climatic glacial/interglacial oscillations and the astronomical forcing. For doing so, a series of appropriate concepts and tools have been developed. A van der Pol-type relaxation oscillator, designed to reproduce the slow-fast dynamics of the paleoclimatic records, has been used for illustration purposes, but the methodology proposed here may of course be applied to other paleoclimatic models.

To study the uniqueness of synchronization, we proposed a convenient concept of the number of attracting trajectories in the phase space of the nonautonomous forced system, each of which corresponds to a synchronized solution. We computed the number of synchronized solutions using a numerical clustering technique, and uncovered that in addition to a *unique* or *monostable* synchronization, there are parameter settings where one finds a *nonunique* or *multistable* synchronization. At low forcing amplitude we found regions of *mode locking* where the system synchronizes on the individual components of the astronomical forcing in a way that is similar to frequency-locking on periodic forcing (Arnol'd tongues), giving rise to coexisting synchronized solutions. As the forcing amplitude is increased, the combined effects of precession and obliquity restrict the number of possible synchronized solutions. The emerging stability diagram consists of a large region of monostable synchronization mixed with smaller regions of multistable synchronization. A comparison with periodic forcing shows that the system finds it easier to synchronize to quasiperiodic insolation forcing. It is therefore conceivable that the climate system wandered throughout preferential synchronization regimes on obliquity, precession, or combinations of both, as environmental parameters varied throughout the history of the Pleistocene.

The robustness of generalized synchronization was investigated in terms of the key indicators of stability of synchronized solutions: the long- and short-term largest Lyapunov exponent (local stability), and the geometry of the basins of attraction (global stability). We found that even though the synchronized solutions are locally stable on a long term, there exists episodes where the short-term largest Lyapunov exponent becomes positive, leading to temporary desynchronizations. As a result, climatic trajectories could diverge from the synchronized solution for some period of time (50 kyr typ-

ically). Moreover, we computed the evolving shape of the basins of attraction for the coexisting synchronized solutions, and uncovered that these solutions sometimes approach the basin boundary where they become very susceptible to external perturbations. As a result, a small perturbation could make the climate jump from one synchronized solution to another, reducing predictability. Such jumps seem to be most likely when the temporary loss of the local stability coalesces with the proximity to the basin boundary. In this context, we briefly discussed the effect of stochastic perturbations on the timing of the deglaciations. We also illustrated the difference between the evolving shape of the basins of attraction for periodic and quasiperiodic insolation forcing. In the case of the insolation forcing, we obtained an intricate pattern of basins of attraction that does not appear to repeat itself in time.

Acknowledgements

We are grateful to Guillaume Lenoir for his thorough review of the several versions of the paper. The original idea of using clustering analysis for automatically identifying the number of stable locking states came to the main author, after presentations and discussions, especially at the 1st ITOP Workshop, held on 23–26 February, 2010 in Marche-en-Famenne, Belgium, and also from the 458. WE-Heraeus-Seminar on ‘SYNCLINE 2010: Synchronization in Complex Networks’, held on 26–29 May 2010 at the Physikzentrum Bad Honnef (Germany), where some preliminary results of this research have been presented in a poster [De Saedeleer et al., 2010]. The project is funded by the ERC (European Research Council) starting grant ITOP (‘Integrated Theory and Observations of the Pleistocene’) under the convention ERC-2009-5tg 239604-ITOP. M. Crucifix is Research Associate with the Belgian National Fund of Scientific Research, and B. De Saedeleer is Post Doctoral Research Assistant with the ITOP Project. Some Figures and calculations where made with the R language and the Intel Fortran Compiler.

Appendix

A Insolation model using 35 terms

We give at the Table 1 the numerical values of the 3×35 terms for computing the insolation $F(t)$ following Eq. (1) in Sect. 1.

Table 1: Coefficients for the insolation model described in Eq. (1) used for the incoming solar radiation anomaly at Summer Solstice and at 65°N . The first 15 terms correspond to the obliquity component, while the other 20 terms correspond to the precession.

ω_i [rad/kyr]	s_i [W/m ²]	c_i [W/m ²]
0.153249478547167	-11.2287376815124	3.51682075211241
0.158148666238883	-3.82499371467540	-0.761851750263805
0.117190147169570	2.28814805956066	1.80233702684623
0.155061775112933	-1.29770081956440	-0.635152963728496
0.217333905941751	0.380973541305497	-1.46301711999210
0.150162587421217	1.54904176353302	-0.0883941912769817
0.211709630908568	-0.810768209286259	-0.577980646565494
0.156336369673117	-0.918358442095885	0.196083726889428
0.148350290855451	0.256895610735773	-0.524697312305024
0.206924898030688	-0.335783913402678	-0.0194792150128644
0.212525165090383	0.267659228540196	0.128915417116900
0.229992875969202	0.0696189733188958	0.0746231714061285
0.306498957094334	0.0247349748169616	0.0140464395340974
0.311398144786051	0.0138353727621181	0.0304736668840422
0.004899187691716	-0.160479848721994	0.0594077968934257
0.264933601588513	-15.5490493322904	-9.70406287110532
0.280151350350945	15.4319556361701	4.75247271131525
0.331110950251899	9.0992249352734	-10.6115244887390
0.328024059125949	-7.87065384013669	6.61544246063503
0.326211762560183	0.813786144754451	-4.52641408099246
0.269742342439881	0.0690448504314857	-3.31639260969558
0.332923246817665	1.44050770785967	1.06339286050120
0.371638925683567	0.925324276580528	-1.02066758672154
0.275366617473065	0.997628846513796	-0.362906496840039
0.323124871434233	-0.378637986107629	0.527217891742183
0.259396912994958	0.339477750517033	-0.560509461538342
0.324937167999999	-0.576082669762308	1.18669572739338
0.334197841377850	0.346906064369828	-0.648189701487285
0.274551083291250	-0.441772417569753	0.289576210423804
0.418183080135680	-0.0184884064645011	0.109632390175297
0.111684123041346	-0.428006728186239	0.357006342316690
0.433400828898112	-0.0049199219454561	-0.106148873639336
0.126901871803777	0.257509918217341	-0.377639794223366
0.336010137943616	-0.421809264016129	0.324327509437558
0.177861471704732	-0.161827722328271	-0.362683869407858

B The classical van der Pol oscillator : description and dynamical behaviour

Classical van der Pol oscillator

The classical van der Pol oscillator [van der Pol, 1926] is very well known, widely used and deeply studied; here the necessary description which is relevant to the scope of this article is given. For more details the reader is referred to the literature, see e.g. [Strogatz, 1994].

This van der Pol-type oscillator model can be regarded as a special case of the FitzHugh-Nagumo (FHN) model [Kosmidis and Pakdaman, 2003], also known as Bonhoeffer-van der Pol (BVP) model [Barnes and Grimshaw, 1997].

Historically, this model was derived by van der Pol, when he discovered the existence of oscillations in electrical circuits. He found that the oscillation period is determined by $\tau^* = RC$ (time constant of relaxation) in RC circuits, or by $\tau^* = L/R$ in RL circuits; hence he named this oscillation as *relaxation oscillations*. The interesting characteristics of the relaxation oscillation are the slow asymptotic behavior and the sudden discontinuous jump to another value. This oscillator has therefore been widely used in many fields like in physical and biological sciences, neurology, seismology, lasers, optoelectronics, etc.

This two-dimensional system exhibits the same basic dynamical features (limit cycle and slow-fast dynamics) necessary to fit the paleoclimatic data, except the asymmetry, for which the system will be corrected for, by the introduction of an additional parameter β (see Eq. 4a in Sect. 1).

This van der Pol oscillator is non conservative with a nonlinear damping, governed by the following second-order differential equation [Balanov et al., 2009] — in the case without forcing :

$$\ddot{x} - \mu(1 - x^2)\dot{x} + x = 0 \quad (\text{B.1})$$

where $\mu > 0$ is a positive constant proportional to the damping.

The van der Pol oscillator is a Liénard system [Strogatz, 1994], because $f(x) = -\mu(1 - x^2)$ is an even function and because $g(x) = x$ is an odd function (see Eq. B.1), in the canonical form :

$$\ddot{x} + f(x)\dot{x} + g(x) = 0 \quad (\text{B.2})$$

Moreover, since this Liénard system satisfies additionally the Liénard theorem, it has a unique and stable limit cycle¹² in the phase space surrounding the origin. This is a feature which is absolutely required in order to model the glacial-interglacial oscillations.

By way of the Liénard transformation $y = x - x^3/3 - \dot{x}/\mu$, the second-order Eq. B.1 can be transformed into an equivalent two-dimensional system of ODE's :

$$\dot{x} = \mu(x - x^3/3 - y) \quad (\text{B.3})$$

$$\dot{y} = x/\mu \quad (\text{B.4})$$

which can also be expressed under the equivalent following form (using the convention $\varepsilon = -1/\mu$, so that $\varepsilon \rightarrow 0$ means more and more damping):

$$\dot{x} = (y - \Phi'(x))/\varepsilon \quad (\text{B.5})$$

$$\dot{y} = -\varepsilon x \quad (\text{B.6})$$

introducing the function $\Phi'(x)$:

$$\Phi'(x) = x^3/3 - x \quad (\text{B.7})$$

the associated potential $\Phi(x)$ having the shape of a 2-well potential. By varying ε , we can adjust the respective time scales of the x and y variables; for $\varepsilon < 1$, the slow-fast variable is x and the slow variable is y . Note that in the main body of this paper, x and y are inverted, so that x will represent the slowly varying ice volume (see Fig. 4), as it is the classical convention for the dynamical theory of paleoclimates.

When $\mu > 0$, the system exhibits a stable limit cycle, where energy is conserved. Near the origin $x = \dot{x} = 0$, the system is unstable and energy is gained, and far from the origin the system is damped and energy is lost (while when $\mu = 0$, there is no damping, the solution is a pure harmonic signal, and there is conservation of energy everywhere).

There is only one fixed point which is the origin $(x, \dot{x}) = (0, 0)$.

When x is small, $f(x) \approx -\mu$ (negative damping). Thus, the fixed point $(x, \dot{x}) = (0, 0)$ is unstable (an unstable focus when $0 < \mu < 2$, and an unstable node otherwise); see [Hilborn, 2000]. On the other hand, when x is large, $f(x) \approx +\mu x^2$ (positive damping). Therefore, the dynamics of the system is expected to be restricted in some area around the fixed point.

¹² The nowadays still unsolved Hilbert's 16th Problem is related to determining the number and location of limit cycles for an autonomous planar vector field for which both functions are real polynomials of fixed degree.

When $0 < \mu \ll 1$ (small damping), the system can be rewritten in order to avoid division by μ . When $\mu \gg 1$ (large damping), the oscillations become less and less symmetric.

When driven, the van der Pol oscillator can lead to synchronization [Balanov et al., 2009], but also to deterministic chaos [Ruihong et al., 2008], depending of the level of the driving force. Since the paleoclimatic system is driven by the insolation, one could also have synchronization and perhaps chaos – or at least some path on the routes leading to chaos; i.e. Lyapunov exponents becoming positive.

This oscillator, or slightly different versions of it (a similar one is the Poincaré oscillator [Glass and Sun, 1994]), has been mathematically largely studied under many aspects: bifurcation structure [Metin et al., 1993], fixed points and Arnol'd tongues, chaotic dynamics [Chen and Chen, 2008, Parlitz and Lauterborn, 1987], additive noise [Degli Esposti Boschi et al., 2002], basins of attraction [Barnes and Grimshaw, 1997], etc. In this article, we focus on the synchronization, multistability and predictability properties of a slightly modified version of the classical van der Pol oscillator.

But there is also a big difference of frameworks: usually, a simple periodic forcing is considered, while in the case of the astronomical forcing, the forcing has a much more complex form (quasiperiodic), like the one given in Eq. (1).

Time spent on the slow manifold

In the case of large damping ($\mu \gg 1$, or $\varepsilon \rightarrow 0$), the oscillations become less and less symmetric, and significant differences becomes to appear between τ_{slow} and τ_{fast} , as defined in Section 1.

One can more precisely characterize the slow-fast dynamics of the system by considering Eqs. B.5–B.6. We see that we have in any case $|\dot{y}| \sim \varepsilon$, which means that y is always slow.

When the system is away from the curve $y = \Phi'(x)$, we have $(|\dot{x}| \sim 1/\varepsilon) \gg (|\dot{y}| \sim \varepsilon)$: the vector field is mostly horizontal. And the travel speed is $v = \sqrt{|\dot{x}|^2 + |\dot{y}|^2} \sim 1/\varepsilon \gg 1$, so that the system moves *quickly* in the horizontal direction (y is the slow variable, and x is the slow-fast variable). If $y > \Phi'(x)$, then $\dot{x} > 0$, and the trajectory moves clockwise. See Fig. 4 for an illustration and [Strogatz, 1994] for a discussion about the separation between the two time scales.

When the system enters the region¹³ where $|y - \Phi'(x)| \sim \varepsilon^2$, we then have $(|\dot{x}| \sim \varepsilon) \sim (|\dot{y}| \sim \varepsilon)$: $|\dot{x}|$ and $|\dot{y}|$ are about the same order of magnitude, and the travel speed is $v \sim \varepsilon \rightarrow 0$: the system moves slowly along the curve $y = \Phi'(x)$, and eventually exits from this region, and so on: the system has a stable limit cycle.

Hence we have the following relationships:

$$\tau_{slow} \sim \mu \quad \text{or} \quad \tau_{slow} \sim 1/\varepsilon \quad (\text{B.8})$$

$$\tau_{fast} \sim 1/\mu \quad \text{or} \quad \tau_{fast} \sim \varepsilon \quad (\text{B.9})$$

The period of the oscillations (or of the unperturbed limit cycle), given by

$$T_{Cycle} = \tau_{slow} + \tau_{fast} \quad , \quad (\text{B.10})$$

is mainly determined by the time during which the system stays around the curve $y = \Phi'(x)$, which can be roughly estimated to be $T \propto 1/\varepsilon$, as $v \sim \varepsilon \rightarrow 0$. So, the larger the damping (lower ε), the longer the period of the oscillations; that's why an additional time scaling (factor τ) must sometimes be done in order to keep the 100 kyr period for the limit cycle (see Fig 4).

Let us mention also that analytical expressions have been derived for the amplitude and period of the limit cycle [D'Acunto, 2006] in both cases (μ small or big), and also for the slow manifold equation [Ginoux and Rossetto, 2006]. There exists also a very fast transition upon variation of a parameter β , from a small amplitude limit cycle to a large amplitude relaxation cycle, explained by the so-called canard phenomenon, cycles, and explosion [Benoît et al., 1981, Guckenheimer et al., 2000, Guckenheimer and Haiduc, 2005].

C Technical details about the calculation of the Lyapunov exponents

We first refer the reader to the seminal papers [Shimada and Nagashima, 1979, Benettin et al., 1980]. The methods for computing the Lyapunov (Characteristic) Exponents (LCE) vary depending on the fact that one wishes to achieve the full spectrum of the LCE [Wolf et al., 1985], or only the

¹³This region is sometimes called "boundary layer" [Guckenheimer and Holmes, 1983], by analogy with Fluid Dynamics.

largest one [Rosenstein et al., 1993]. Analytical derivations of the LCE's of the van der Pol oscillator do also exist [Grasman et al., 2005]. In this research, we computed λ_{max} using the standard method involving a Gram-Schmidt Reorthonormalization (GSR) of the 'tangent vectors' [Shimada and Nagashima, 1979, Benettin et al., 1980, Wolf et al., 1985]; which is described in the review paper [Ramasubramanian and Sriram, 2000].

We remind here the fundamental principles. Consider an n -dimensional continuous-time dynamical system :

$$\frac{d\vec{Z}}{dt} = \vec{f}(\vec{Z}, t) \quad (C.1)$$

where \vec{Z} and \vec{f} are n -dimensional vector fields. To determine the LCE's corresponding to some initial condition $\vec{Z}(0)$, we have to find the long term evolution of the axes of an infinitesimal sphere of states around $\vec{Z}(0)$. That is to say that we assume [Ott, 2002] $\delta\vec{Z}(t) = \delta\vec{Z}(0) e^{\Lambda t}$, with $\Lambda = \text{diag}(\lambda_1, \dots, \lambda_n)$, where λ_i are the eigenvalues of the system. For this, we consider the linearization of Eq. C.1, given by:

$$\frac{d\delta\vec{Z}}{dt} = \vec{J} \delta\vec{Z} \quad (C.2)$$

where \vec{J} is the $n \times n$ Jacobian matrix defined by $J_{ij} = \partial f_i / \partial Z_j$. Then, starting from a unit vector $\delta\vec{Z}(0)$, the original system given by Eq. C.1 is integrated for \vec{Z} together with the $\delta\vec{Z}$ tangent system given by Eq. C.2. The evolution of $\delta\vec{Z}$ is such that it tends to align with the most unstable direction (the most rapidly growing one). The choice of the initial vector of the tangent manifold may influence the convergence, but in practice a spin-up phase can be performed in order to find the good direction.

The largest Lyapunov exponent λ_{max} is then defined as :

$$\lambda_{max} = \lim_{|\delta\vec{Z}(0)| \rightarrow 0} \lim_{t \rightarrow \infty} \frac{1}{t} \ln \frac{|\delta\vec{Z}(t)|}{|\delta\vec{Z}(0)|} \quad (5)$$

It is of course impossible in practice to go to infinity¹⁴; so the computation is always truncated to some finite final time, usually of the order of 10^4 – 10^5 times the period of the forcing. The convergence can be more rapidly achieved if some transient behaviour is skipped (like illustrated in Fig. 17), i.e. we compute the LCE's

¹⁴The proof of the existence of such a limit has been made by [Oseledec, 1968].

only when we are quite sure to be on the attracting trajectory.

Note that there exists a whole spectrum of Lyapunov exponents λ_i ($i = 1, 2, \dots, n$), that can be computed with a unit vector basis, and with a renormalization procedure. Although we are mostly interested in λ_{max} in this article — a positive λ_{max} is associated to a desynchronization —, our subroutine allows to compute all the spectrum of λ_i 's of any system. For the sake of flexibility, we used a symbolic software, so that the model could be very easily changed, and all functions (like the Jacobian matrix) are automatically derived once the initial system is given.

One of the standard and popular methods to compute the Lyapunov spectrum of a dynamical system involves a Gram-Schmidt Reorthonormalization (GSR) of the 'tangent vectors' [Shimada and Nagashima, 1979, Benettin et al., 1980, Wolf et al., 1985]; differential versions of this have also been formulated. Our subroutine includes the GSR procedure, which is required in order to avoid computational overflows, and degeneracy into a single vector. The frequency of reorthonormalization is not critical; as a rule of thumb, GSR is usually performed on the order of once per characteristic period. Here, the normalization time step has been chosen optimally, that is to say the largest possible which preserves the accuracy. Since the GSR never affects the direction of the first vector in a system, this vector tends to seek out the direction in tangent space which is most rapidly growing.

Our subroutine has been validated by comparing our LCE's to those of [Ramasubramanian and Sriram, 2000] for several systems (driven van der Pol, Lorenz '63, etc.); the order of the accuracy achieved is 1‰ for the Lorenz system¹⁵. One also checked that $\text{div } \vec{f} = \text{Tr}(\vec{J}) = -\sigma - 1 - \beta = -13.66 = \sum_{i=1}^n \lambda_i$ holds.

Coming back to our system of Eqs 4a–4b, for which the Jacobian matrix is:

$$\vec{J} = - \begin{bmatrix} 0 & 1 \\ -\alpha & \alpha\Phi''(y) \end{bmatrix} / \tau = \vec{J}(y, \alpha) \quad (C.3)$$

we end up to the following results (Fig. 17): the system Eq. (4) subject to the insolation (Eq. (1)) is synchronized on a long term, since $\lambda_{max} = -0.2 \text{ kyr}^{-1} < 0$.

¹⁵For the Lorenz system, one must pay attention to the spurious trivial set of LCE's corresponding to the origin [Shimada and Nagashima, 1979, Bryant et al., 1990].

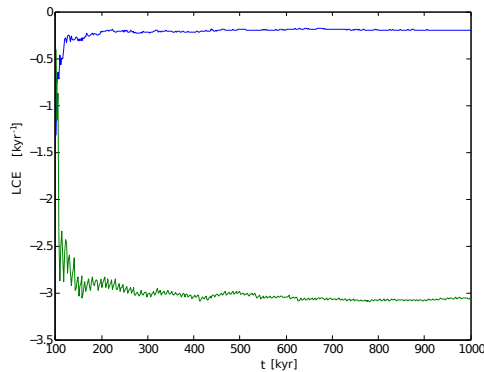


Figure 17: Convergence of the two LCE's of one of the two attracting trajectories of the system Eq. (4), subject to the insolation (Eq. (1)); some transient is skipped. For $\tau = 3.33$, we have $\lambda_{max} = -0.2 \text{ kyr}^{-1} < 0$ (for $\tau = 35.09$, the value must be scaled accordingly, which would give -0.019 kyr^{-1}), so the system is synchronized on a long term.

Some properties of the LCE's (λ_i)

The LCE's are very useful in order to characterize the dynamical behaviour of a system; for example, here are a few interesting properties, valid in the case of the dissipative system Eq. (4) in the autonomous case :

- a dynamical system of dimension n has n LCE's and n eigenvectors [Lichtenberg and Lieberman, 1983],
- $\sum_{i=1}^n \lambda_i = \text{Tr}(\vec{J}) = \text{div } \vec{f}$, both being related to the growth of a volume of dimension n of the phase space [Shimada and Nagashima, 1979],
- $\text{div}(\vec{f}) < 0$ for a dissipative system (hence the system has at least one negative exponent),
- $\lambda_i = 0$ along a limit cycle (tangent direction of the attractor) [Kantz and Schreiber, 2004],
- at least one LCE vanishes if the trajectory of an attractor does not contain a fixed point [Haken, 1983],
- the nature of the attractor can be described by analyzing the sign of the LCE's, which gives a qualitative picture of the dynamics [Wolf et al., 1985, Müller, 1995], also function of the dimension (1D to 4D), e.g. an attractor for a dissipative system

with one or more $\lambda_i > 0$ is said to be *strange* or *chaotic*; if more than one $\lambda_i > 0$, there is *hyperchaoticity* [Rossler, 1979].

- the existence of $\lambda_i > 0$ is mathematically related to the theory of ergodicity¹⁶ of dynamical systems [Eckmann and Ruelle, 1985],
- local bifurcations can be detected by detecting changes of signs of λ_i .

The LCE spectrum is closely related to the fractional dimension of the associated strange attractor by the Kaplan-Yorke formula [Kaplan and Yorke, 1979]. There are a number of similar measures of the "strangeness" of strange attractors, like the fractal dimension [Theiler, 1990], information dimension, box-counting dimension, and the correlation dimension [Tsiganis et al., 1999] and exponent [Grassberger and Procaccia, 1983], which allows to distinguish between deterministic chaos and random noise, and is computationally easier.

It is also possible to estimate the LCE of a system by analyzing its time series, but with limited data, or a system subject to non negligible stochastic perturbation, the classical methods may provide incorrect or ambiguous results [Ruelle, 1990], hence require specific methods, like [McCaffrey et al., 1992, Liu et al., 2005].

D Technical details about the computation of the basins of attraction

The practical computation of a basin of attraction is done as follows.

Let us for example come back to the Fig. 5(e), with the three attracting trajectories $AT_i(x, y, t)$ due to the insolation forcing.

Now, we wonder which initial condition leads ultimately to which of the three AT_i . This is the concept of the *basin of attraction* of a given AT_i , classically defined by the set of states that leads to a given AT_i . Let us more precisely define the basin of attraction of a given

¹⁶An attractor is said *ergodic* (or *transitive*) if the points fill an entire physically realizable domain; *intransitive* if there are distinct attractors in several closed subdomains [Saltzman, 2002], and a system is *almost intransitive* if it resides for long periods of time in one or another domain that is not fully closed off, so that occasional exits from one domain to another can occur.

AT_i as the locus of all points in the (x, y) plane which lead to motion which ultimately converges on that AT_i .

We initialize many initial conditions on a fine rectangular grid covering the phase space. Each initial condition is then integrated forward to see which AT_i its trajectory approached. If the trajectory approached a particular one of the three AT_i 's, a dot coloured by the color identifying the AT_i is plotted on the grid. For doing this, we need to define a target time at which we will do the classification, and a criteria for the classification.

The classification algorithm is illustrated in Fig. 18, where a cut has been made at a target time $t = 550$ kyr. The three AT_i 's are displayed, together with the location of the trajectories (black circles). To decide if a given trajectory ends up onto a given AT_i , we choose a maximum distance from the AT_i (dotted circle); taken here to be $1/4$ of the minimum distance between two AT_i 's. Trajectories falling into that dotted circle are classified as ending into AT_i .

We consider a given trajectory starting from $t_0 = 0$ kyr, integrate it up to $t = 550$ kyr, and then we examine its position with respect to the AT_i at the same time $T=550$ kyr. If the distance to a given AT_k is 'sufficiently small' (see the circles around the AT_i), then this initial condition is coloured in the k^{th} color, associated with the k^{th} attracting trajectories AT_i .

Repeating this process for each initial condition on a fine grid of the whole phase space gives the shape of the basins of attraction. As we have three attracting trajectories, we will have three basins of attraction. Such basins of attraction obtained are shown in Fig. 19.

As we are in the case of a non-autonomous system, we then have to repeat this procedure for several starting times t_0 (the position of the AT_i 's are constantly evolving, hence the shape of the basins are also varying with time). This has been done to produce the evolving shape of the basins of attraction in Figs. 11 and 12.

Note that if t is too close from t_0 , transient behaviours predominate, and not enough time has elapsed in order for the trajectory to be attracted by a given AT_i , hence the basins of attraction cannot be defined in that case.

The glacial/interglacial cycles do exist since about 3 million years, but only 8 limit cycles of 100 kyr period have been performed, since the Mid-Pleistocene Transition (MPT). This should however be sufficient to converge onto the attracting trajectories, because the climatic trajectories are rapidly attracted on the limit cycle. So, if the ice age model Eq. (4) is a realistic one, it would be reasonable to state that the transient of climate dynamics has gone, and that we are currently probably

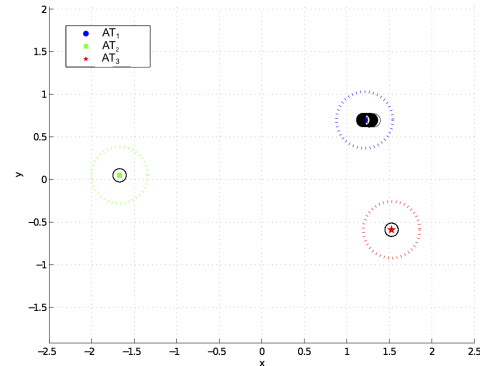


Figure 18: Illustration of the classification algorithm, which allows to compute the basins of attractions. The position of the 70 trajectories (black circles) with respect to the three attracting trajectories (symbols) at time $t = 550$ kyr, starting from $t_0 = 20$ kyr, are shown. If the trajectory falls into a dotted circle, classification is possible. The 70 trajectories form three highly concentrated clusters, corresponding to the three attracting trajectories.

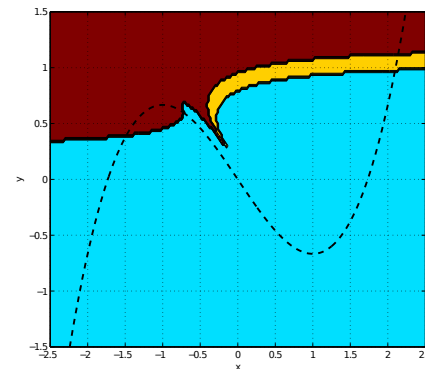


Figure 19: When integrating the system system Eq. (4), with many initial conditions (grid $201 \times 121 = 24\,321$) starting from time $t_0 = 0$ kyr, with the insolation forcing given by Eq. (1), we obtain the three basins of attraction above; each basin is coloured with the colour of the corresponding AT_i . The function $\Phi'(y) = y^3/3 - y = x$, corresponding to the slow manifold, is also shown (dashed curve).

somewhere on an attracting trajectory, if any.

E Instantaneous stability

As we considered the long-term (3 Myr) and short-term ($H = 50$ kyr) local stabilities, we could wonder why not to consider also, at the other extreme, the 'very short-term' local stability ($H \rightarrow 0$). Even if it has probably less relevance in the context of predictability of glaciations, it may however still be computed and understood as an *instantaneous* stability. As the horizon of time H tends to zero, it means that we no longer consider any motion in the phase space (no average in time), hence the instantaneous stability becomes also a local property in the phase space.

The same formula (Eq. 6) as for the short-term stability is used, but now with an Horizon of $H = 1$ kyr, representing the very short-term. The result is plotted in Fig. 20, where the trajectory has been coloured with the $\lambda_{max}^{H=1}$ values. There are black areas, which means local instantaneous instability. This black zone is always in the same region of the phase space: when y lies within the interval $I^* = [-1, 1]$, whatever the initial condition.

We now demonstrate mathematically why the black zone in Fig. 20 *left* is located within the interval $I^* = [-1, 1]$.

Let us derive the theoretical expression of the exactly instantaneous LCE λ_i^{inst} . If we call Λ_i the eigenvalues of the jacobian matrix J , then the λ_i^{inst} are defined as $\lambda_i^{inst} = \lim_{t \rightarrow 0} \frac{1}{t} \ln \Lambda_i$ [Drazin and King, 1992], so that we can obtain the largest λ_i^{inst} by computing $\lambda_{max}^{inst} = \max(\Re(\Lambda_i))$.

As the Jacobian matrix J is a function of y only (and not x), see Eq. C.3, so do λ_{max}^{inst} . The function $\lambda_{max}^{inst}(y)$ is plotted (Fig. 20, *right*, black dotted curve), where we clearly see that it is positive on the interval $[-1, 1]$, which is precisely the same interval as I^* .

□

Moreover, the numerical values also match (e.g. the maximum of the function λ_{max}^{inst} has a value of about 0.28, which correspond to the maximum of the color scale).

An interpretation of λ_{max}^{inst} is that a particular trajectory makes a travel through the phase space 'painted' by λ_{max}^{inst} , integrating so the instantaneous stability to achieve the short-term and long-term stabilities.

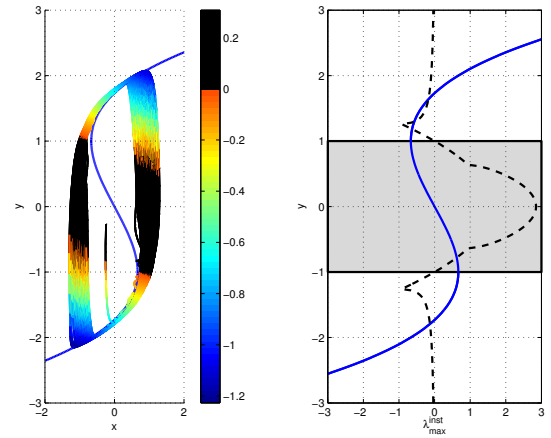


Figure 20: Very short-term stability. *Left* : the attracting climatic trajectory (initial conditions $(x_0, y_0) = (-0.24, -0.27)$) is coloured by the values of $\lambda_{max}^{H=1}$ for the system Eq. (4) with $\alpha = 11.11$, $\beta = 0.25$, $\gamma = 0.033$ and $\tau = 35.09$. Instantaneous instability ($\lambda_{max}^{H=1} > 0$) occurs for $y \in I^* = [-1, 1]$. *Right*: the function $10 \times \lambda_{max}^{inst}$ (black dashed curve) has positive values for the same range $y \in I^* = [-1, 1]$. For both graphs, the function $\Phi'(y) = x$ has been superimposed for an improved reading and easier interpretation.

References

- [Abarbanel et al., 1991] Abarbanel, H. D. I., Brown, R., and Kennel, M. B. (1991). Variation of lyapunov exponents on a strange attractor. *Journal of Nonlinear Science*, 1(2):175–199.
- [Abarbanel et al., 1996] Abarbanel, H. D. I., Rulkov, N. F., and Sushchik, M. M. (1996). Generalized synchronization of chaos: The auxiliary system approach. *Phys. Rev. E*, 53(5):4528–4535.
- [Arnold, 1983] Arnold, V. (1983). *Geometrical Methods in the Theory of Ordinary Differential Equations*. Springer-Verlag, New York, 1988 second edition. English translation of the original russian publication: "Dopolnitel'nye Glavy Teorii Obyknovennykh Differentsial'nykh Uravnenii" (Additional Chapters to the Theory of Ordinary Differential Equations, Moscow: Nauka, 1978).
- [Ashkenazy, 2006] Ashkenazy, Y. (2006). The role of phase locking in a simple model for glacial dynamics. *Climate Dynamics*, 27(4):421–431.
- [Balanov et al., 2009] Balanov, A., Janson, N., Postnov, D., and Sosnovtseva, O. (2009). *Synchronization: From Simple to Complex*. Springer-Verlag, Berlin, Germany.
- [Barnes and Grimshaw, 1997] Barnes, B. and Grimshaw, R. (1997). Analytical and numerical studies of the bonhoeffer van der pol system. *The ANZIAM Journal*, 38(04):427–453.
- [Belogortsev, 1992] Belogortsev, A. B. (1992). Quasiperiodic resonance and bifurcations of tori in the weakly nonlinear duffing oscillator. *Physica D: Nonlinear Phenomena*, 59(4):417–429.
- [Benettin et al., 1980] Benettin, G., Galgani, L., Giorgilli, A., and Strelcyn, J.-M. (1980). Lyapunov characteristic exponents for smooth dynamical systems and for hamiltonian systems; a method for computing all of them. part 2: Numerical application. *Meccanica*, 15(1):21–30.
- [Benoît et al., 1981] Benoît, E., Callot, J., Diener, F., and Diener, M. (1981). Chasse au canard. *Colloctanea Mathematica*, 31-32(1-3):37–119.
- [Berger, 1978] Berger, A. L. (1978). Long-term variations of daily insolation and Quaternary climatic changes. *J. Atmos. Sci.*, 35:2362–2367.
- [Broecker and van Donk, 1970] Broecker, W. S. and van Donk, J. (1970). Insolation changes, ice volumes, and the O18 record in deep-sea cores. *Rev. Geophys.*, 8(1):169–198.
- [Broer and Simó, 1998] Broer, H. W. and Simó, C. (1998). Hill's equation with quasi-periodic forcing: resonance tongues, instability pockets and global phenomena. *Soc. Brasil Mat.*, (29):253293.
- [Brown and Kocarev, 2000] Brown, R. and Kocarev, L. (2000). A unifying definition of synchronization for dynamical systems. *Chaos*, 10(2):344–349.
- [Bryant et al., 1990] Bryant, P., Brown, R., and Abarbanel, H. D. I. (1990). Lyapunov exponents from observed time series. *Physical Review Letters*, 65(13).
- [Chen and Chen, 2008] Chen, J.-H. and Chen, W.-C. (2008). Chaotic dynamics of the fractionally damped van der pol equation. *Chaos, Solitons & Fractals*, 35(1):188–198.
- [Crucifix, 2011] Crucifix, M. (2011). Oscillators and relaxation phenomena in Pleistocene climate theory. *Transactions of the Philosophical Transactions of the Royal Society (Series A, Physical Mathematical and Engineering Sciences)*, In Press.
- [D'Acunto, 2006] D'Acunto, M. (2006). Determination of limit cycles for a modified van der pol oscillator. *Mechanics Research Communications*, 33(1):93–98.
- [De Saedeleer et al., 2010] De Saedeleer, B., Crucifix, M., and Wieczorek, S. (2010). Is the synchronization of the climatic system on the orbital forcing robust? Poster presented at the "SYNCLINE 2010: Synchronization in Complex Networks" conference, held on 26–29 May 2010 at the Physikzentrum Bad Honnef (Germany).
- [Degli Esposti Boschi et al., 2002] Degli Esposti Boschi, C., Ortega, G. J., and Louis, E. (2002). Discriminating dynamical from additive noise in the van der pol oscillator. *Physica D: Nonlinear Phenomena*, 171(1-2):8–18.
- [Dijkstra et al., 2003] Dijkstra, H. A., Weijer, W., and Neelin, J. D. (2003). Imperfections of the three-dimensional thermohaline circulation: hysteresis and unique-state regimes. *J. Phys. Oceanogr.*, 33:2796–2814.

- [Doedel et al., 2009] Doedel, E., Champneys, A., Dercole, F., Fairgrieve, T., Kuznetsov, Y., Oldeman, B., Paffenroth, R., Sandstede, B., Wang, X., and Zhang, C. (2009). Auto: Software for continuation and bifurcation problems in ordinary differential equations. Technical report, Montreal.
- [Donges et al., 2009] Donges, J. F., Zou, Y., Marwan, N., and Kurths, J. (2009). The backbone of the climate network. *EPL (Europhysics Letters)*, 87(4):48007.
- [Drazin and King, 1992] Drazin, P. G. and King, G. P., editors (1992). *Interpretation of Time Series from Nonlinear Systems*, volume 58.
- [Eckmann and Ruelle, 1985] Eckmann, J. P. and Ruelle, D. (1985). Ergodic-theory of chaos and strange attractors. *Reviews of Modern Physics*, 57(3):617–656.
- [Ginoux and Rossetto, 2006] Ginoux, J.-M. and Rossetto, B. (2006). Differential geometry and mechanics: Applications to chaotic dynamical systems. *I. J. Bifurcation and Chaos*, 16(4):887–910.
- [Glass and Sun, 1994] Glass, L. and Sun, J. (1994). Periodic forcing of a limit-cycle oscillator: Fixed points, Arnold tongues, and the global organization of bifurcations. *Phys. Rev. E*, 50:5077–5084.
- [Glendinning and Wiersig, 1999] Glendinning, P. and Wiersig, J. (1999). Fine structure of mode-locked regions of the quasi-periodically forced circle map. *Physics Letters A*, 257(1-2):65–69.
- [Grasman et al., 2005] Grasman, J., Verhulst, F., and Shih, S. (2005). The Lyapunov exponents of the Van der Pol oscillator. *Mathematical Methods in the Applied Sciences*, 28:1131–1139.
- [Grassberger and Procaccia, 1983] Grassberger, P. and Procaccia, I. (1983). Measuring the strangeness of strange attractors. *Physica D: Nonlinear Phenomena*, 9(1-2):189–208.
- [Guckenheimer and Haiduc, 2005] Guckenheimer, J. and Haiduc, R. (2005). Canards at folded node. *Mosc. Math. J.*, 5:91–103.
- [Guckenheimer et al., 2000] Guckenheimer, J., Hoffman, K., and Weckesser, W. (2000). Numerical computation of canards. *International Journal of Bifurcation and Chaos*, 10(12):2269–2687.
- [Guckenheimer and Holmes, 1983] Guckenheimer, J. and Holmes, P. (1983). *Nonlinear oscillations, dynamical systems, and bifurcations of vector fields*. Springer-Verlag, New York.
- [Haken, 1983] Haken, H. (1983). At least one lyapunov exponent vanishes if the trajectory of an attractor does not contain a fixed point. *Physics Letters A*, 94(2):71–72.
- [Hays et al., 1976] Hays, J. D., Imbrie, J., and Shackleton, N. J. (1976). Variations in the Earth's orbit : Pacemaker of ice ages. *Science*, 194:1121–1132.
- [Hilborn, 2000] Hilborn, R. (2000). *Chaos and Nonlinear Dynamics: an Introduction for Scientists and Engineers*. Oxford University Press.
- [Huybers, 2007] Huybers, P. (2007). Glacial variability over the last two millions years: an extended depth-derived age model, continuous obliquity pacing, and the Pleistocene progression. *Quaternary Sci. Rev.*, 26:37–55.
- [Imbrie and Imbrie, 1980] Imbrie, J. and Imbrie, J. Z. (1980). Modelling the climatic response to orbital variations. *Science*, 207:943–953.
- [Kantz and Schreiber, 2004] Kantz, H. and Schreiber, T. (2004). *Nonlinear Time Series Analysis*. Cambridge University Press, Cambridge, U.K., 2nd edition.
- [Kaplan and Yorke, 1979] Kaplan, J. L. and Yorke, J. A. (1979). Chaotic behavior of multidimensional difference equations. In *Functional differential equations and approximation of fixed points (Proc. Summer School and Conf., Univ. Bonn, Bonn, 1978)*, volume 730 of *Lecture Notes in Math.*, pages 204–227. Springer, Berlin.
- [Kloeden, 2000] Kloeden, P. E. (2000). A Lyapunov function for pullback attractors of nonautonomous differential equations. *Electronic J. Diff. Eqns, Conf.* 05, pages 91–102.
- [Kosmidis and Pakdaman, 2003] Kosmidis, E. K. and Pakdaman, K. (2003). An analysis of the reliability phenomenon in the fitzhugh-nagumo model. *Journal of Computational Neuroscience*, 14(1):5–22.
- [Langa et al., 2002] Langa, J. A., Robinson, J. C., and Suárez, A. (2002). Stability, instability, and bifurcation phenomena in non-autonomous differential equations. *Nonlinearity*, 15(3):1–17.

- [Laskar et al., 2004] Laskar, J., Robutel, P., Joutel, F., Boudin, F., Gastineau, M., Correia, A. C. M., and Levrard, B. (2004). A long-term numerical solution for the insolation quantities of the Earth. *Astrom. Astroph.*, 428:261–285.
- [Le Treut and Ghil, 1983] Le Treut, H. and Ghil, M. (1983). Orbital forcing, climatic interactions and glaciation cycles. *J. Geophys. Res.*, 88(C9):5167–5190.
- [Lichtenberg and Lieberman, 1983] Lichtenberg, A. J. and Lieberman, M. A. (1983). *Regular and stochastic motion*. Springer-Verlag, New York.
- [Lisiecki and Raymo, 2005] Lisiecki, L. E. and Raymo, M. E. (2005). A pliocene-pleistocene stack of 57 globally distributed benthic $\delta^{18}O$ records. *Paleoceanography*, 20(1).
- [Lisiecki and Raymo, 2007] Lisiecki, L. E. and Raymo, M. E. (2007). Plio-pleistocene climate evolution: trends and transitions in glacial cycle dynamics. *Quaternary Science Reviews*, 26(1-2):56–69.
- [Liu et al., 2005] Liu, H.-F., Dai, Z.-H., Li, W.-F., Gong, X., and Yu, Z.-H. (2005). Noise robust estimates of the largest lyapunov exponent. *Physics Letters A*, 341(1-4):119–127.
- [Luethi et al., 2008] Luethi, D., Le Floch, M., Bereiter, B., Blunier, T., Barnola, J.-M., Siegenthaler, U., Raynaud, D., Jouzel, J., Fischer, H., Kawamura, K., and Stocker, T. F. (2008). High-resolution carbon dioxide concentration record 650,000–800,000 years before present. *Nature*, 453(7193):379–382.
- [Marwan et al., 2009] Marwan, N., Donges, J. F., Zou, Y., Donner, R. V., and Kurths, J. (2009). Complex network approach for recurrence analysis of time series. *Physics Letters A*, 373(46):4246–4254.
- [McCaffrey et al., 1992] McCaffrey, D. F., Ellner, S., Gallant, A. R., and Nychka, D. W. (Sep., 1992). Estimating the lyapunov exponent of a chaotic system with nonparametric regression. *Journal of the American Statistical Association*, 87(419):682–695.
- [Mettin et al., 1993] Mettin, R., Parlitz, U., and Lauterborn, W. (1993). Bifurcation structure of the driven van der pol oscillator. *Int. J. Bifurcation & Chaos*, (3):1529–1555.
- [Milankovitch, 1941] Milankovitch, M. (1941). *Kanon der Erdbestrahlung und Seine Anwendung auf das Eiszeitenproblem (Canon of insolation and the ice-age problem)*. Königl. Serbische Akademie, Belgrad.
- [Müller, 1995] Müller, P. C. (1995). Calculation of lyapunov exponents for dynamic systems with discontinuities. *Chaos, Solitons & Fractals*, 5(9):1671–1681.
- [Oseledec, 1968] Oseledec, V. (1968). A multiplicative ergodic theorem: Ljapunov characteristic numbers for dynamical systems. *Transactions of the Moscow Mathematical Society*, 19:197–231.
- [Osinga et al., 2000] Osinga, H., Wiersig, J., Glendinning, P., and Feudel, U. (2000). Multistability and nonsmooth bifurcations in the quasiperiodically forced circle map. *ArXiv Nonlinear Sciences e-prints*.
- [Ott, 2002] Ott, E. (2002). *Chaos in Dynamical Systems*. Cambridge University Press.
- [Paillard, 1998] Paillard, D. (1998). The timing of pleistocene glaciations from a simple multiple-state climate model. *Nature*, 391:378–381.
- [Paillard and Parrenin, 2004] Paillard, D. and Parrenin, F. (2004). The Antarctic ice sheet and the triggering of deglaciations. *Earth Planet. Sc. Lett.*, 227:263–271.
- [Parlitz and Lauterborn, 1987] Parlitz, U. and Lauterborn, W. (1987). Period-doubling cascades and devil’s staircases of the driven van der pol oscillator. *Physical Review A*, 36(3).
- [Pikovsky et al., 2001] Pikovsky, A., Rosenblum, M., and Kurths, J. (2001). *Synchronization A Universal Concept in Nonlinear Sciences*. Cambridge University Press, New York.
- [Rahmstorf et al., 2005] Rahmstorf, S., Crucifix, M., Ganopolski, A., Goosse, H., Kamenkovich, I., Knutti, R., Lohmann, G., Marsh, R., Mysak, L. A., Wang, Z., and Weaver, A. J. (2005). Thermohaline circulation hysteresis: A model intercomparison. *Geophys. Res. Lett.*, 32(23).
- [Ramasubramanian and Sriram, 2000] Ramasubramanian, K. and Sriram, M. S. (2000).

- A comparative study of computation of lyapunov spectra with different algorithms. *Physica D: Nonlinear Phenomena*, 139(1-2):72–86.
- [Rosenstein et al., 1993] Rosenstein, M. T., Collins, J. J., and Luca, C. J. D. (1993). A practical method for calculating largest lyapunov exponents from small datasets. *Physica D*, (124).
- [Rossler, 1979] Rossler, O. E. (1979). An equation for hyperchaos. *Physics Letters A*, 71(2-3):155–157.
- [Ruelle, 1990] Ruelle, D. (1990). Deterministic chaos: the science and the fiction. *Proceedings of the Royal Society A, London*, (427):241–248.
- [Ruihong et al., 2008] Ruihong, L., Wei, X., and Shuang, L. (2008). Chaos control and synchronization of the ϕ^6 -van der pol system driven by external and parametric excitations. *Nonlinear Dynamics*, 53(3):261–271.
- [Rulkov et al., 1995] Rulkov, N. F., Sushchik, M. M., Tsimring, L. S., and Abarbanel, H. D. I. (1995). Generalized synchronization of chaos in directionally coupled chaotic systems. *Phys. Rev. E*, 51(2):980–994.
- [Saltzman, 2002] Saltzman, B. (2002). *Dynamical Paleoclimatology: Generalized Theory of Global Climate Change (International Geophysics)*. Academic Press.
- [Saltzman et al., 1984] Saltzman, B., Hansen, A. R., and Maasch, K. A. (1984). The late Quaternary glaciations as the response of a 3-component feedback-system to Earth-orbital forcing. *Journal of the Atmospheric Sciences*, 41(23):3380–3389.
- [Saltzman and Maasch, 1990] Saltzman, B. and Maasch, K. A. (1990). A first-order global model of late Cenozoic climate. *Trans. R. Soc. Edinburgh Earth Sci*, 81:315–325.
- [Saltzman and Maasch, 1991] Saltzman, B. and Maasch, K. A. (1991). A first-order global model of late Cenozoic climate. II further analysis based on a simplification of the CO₂ dynamics. *Clim. Dyn.*, 5:201–210.
- [Savi, 2005] Savi, M. A. (2005). Chaos and order in biomedical rhythms. *Journal of the Brazilian Society of Mechanical Sciences and Engineering*, 27(2):157–169.
- [Shimada and Nagashima, 1979] Shimada, I. and Nagashima, T. (1979). A numerical approach to ergodic problem of dissipative dynamical systems. *Progr. Theoret. Phys.*, 61(6):1605–1616.
- [Strogatz, 1994] Strogatz, S. H. (1994). *Nonlinear Dynamics And Chaos: With Applications To Physics, Biology, Chemistry, And Engineering (Studies in Nonlinearity)*. Studies in nonlinearity. Perseus Books Group, 1 edition.
- [Svensson and Coombes, 2009] Svensson, C.-M. and Coombes, S. (2009). Mode locking in a spatially extended neuron model: active soma and compartmental tree. *International Journal of Bifurcation and Chaos*, 19(8):2597–2607.
- [Theiler, 1990] Theiler, J. (1990). Estimating fractal dimension. *J. Opt. Soc. Am. A*, 7(6):1055–1073.
- [Tsiganis et al., 1999] Tsiganis, K., Anastasiadis, A., and Varvoglis, H. (1999). Effective lyapunov numbers and correlation dimensions in a 3-D hamiltonian system. In Henrard, J. and Ferraz-Mello, S., editors, *IAU-Colloquium No 172 - The impact of modern dynamics in Astronomy*, pages 447–448.
- [Tziperman and Gildor, 2003] Tziperman, E. and Gildor, H. (2003). On the mid-Pleistocene transtion to 100-kyr glacial cycles and the asymmetry between glaciation and deglaciation times. *Paleoceanography*, 18(1):1001.
- [Tziperman et al., 2006] Tziperman, E., Raymo, M. E., Huybers, P., and Wunsch, C. (2006). Consequences of pacing the Pleistocene 100 kyr ice ages by non-linear phase locking to Milankovitch forcing. *Paleoceanography*, 21:PA4206.
- [van der Pol, 1926] van der Pol, B. (1926). On relaxation oscillations. *Phil. Mag.*, 2(11):978–992.
- [Wieczorek, 2009] Wieczorek, S. (2009). Stochastic bifurcation in noise-driven lasers and hopf oscillators. *Phys. Rev. E*, 79(3):036209.
- [Wieczorek, 2011] Wieczorek, S. M. (2011). Noise synchronisation and stochastic bifurcations in lasers. <http://arxiv.org/abs/1104.4052>.
- [Wiggins, 2003] Wiggins, S. (2003). *Introduction to Applied Nonlinear Dynamical Systems and Chaos*. Texts in Applied Mathematics. Springer, 2nd edition.

- [Wolf et al., 1985] Wolf, A., Swift, J. B., Swinney, H. L., and Vastano, J. A. (1985). Determining lyapunov exponents from a time series. *Physica D: Nonlinear Phenomena*, 16(3):285–317.
- [Wu et al., 2006] Wu, L., Zhu, S., and Li, J. (2006). Synchronization on fast and slow dynamics in drive-response systems. *Physica D: Nonlinear Phenomena*, 223(2):208–213.